Goal-based error estimation for the multi-dimensional diamond difference and box discrete ordinate (S_N) methods.

R.S. Jeffers[a,b], J. Kópházi[a], M.D. Eaton[a], F. Févotte[b], F. Hülsemann[b], J. Ragusa[c]

[a] *Department of Mechanical Engineering, Imperial College of Science, Technology and Medicine, Prince Consort Road, London SW7 2AZ, UK*

[b] *EDF R&D, EDF Lab Paris-Saclay, 7 Boulevard Gaspard Monge, 91120 Palaiseau, France*

[c] *Texas A&M University, Department of Nuclear Engineering, College Station, Texas 77843, USA*

Abstract

Goal-based error estimation due to spatial discretisation and adaptive mesh refinement (AMR) has previously been investigated for the one dimensional, diamond difference, discrete ordinate (1-D DD-S_N) method for discretising the Neutron Transport Equation (NTE). This paper investigates the challenges of extending goal-based error estimation to multi-dimensions with supporting evidence provided on 2-D fixed (extraneous) source and K_{eff} eigenvalue (criticality) verification test cases.

It was found that extending Hennart's weighted residual view of the lowest order 1-D DD equations to multi-dimensions gave what has previously been called the *box method*. This paper shows how the box method can be extended to higher orders. The paper also shows an equivalence between the higher order box methods and the higher order DD methods derived by Hébert et al. Though, less information is retained in the final solution in the latter case. These extensions allow for the definition of dual weighted residual (DWR) error estimators in multi-dimensions for the DD and box methods. However, they are not applied to drive AMR in the multi-dimensional case due to the various challenges explained in this paper.

1. Introduction

The Neutron Transport Equation (NTE) is a partial-integro-differential equation (PIDE) that describes the average statistical behaviour of a gas of neutral particles migrating through a host medium. The solution of the NTE is the angular flux of neutral particles which is a distribution with respect to 6 different variables that represent position (x, y, z), angle (θ, χ) and energy (E) as well as a function of time (t). The NTE encapsulates all the physical processes that would occur to a gas of neutral particles, which is migrating through a heterogeneous and reactive host medium, such as streaming, absorption, scattering, production and leakage. In this paper we will restrict our attention to two-dimensional (2-D), time-independent (steady-state), mono-energetic, fixed (or extraneous) source and K_{eff} eigenvalue (criticality) problems of interest in the field of nuclear reactor physics.

This paper considers the case where the neutral particles are neutrons in inhomogeneous reactive media. The mono-energetic NTE equation is used and discretised in angle using the discrete ordinate (S_N) method and in space using the diamond difference (DD) method. The S_N method involves solving the transport equation along a discrete set of angles given by a prescribed quadrature scheme. Different methods for estimating the error due to discontinuous Galerkin finite element method (DGFEM) discretisation of the transport equation have been discussed and compared in (Hart and Azmy, 2017). Despite the increased use of finite elements (FE) for spatial discretisation, many full scale production codes use the diamond difference (DD) method for solving the discrete ordinate (S_N) angular discretisation of the neutron transport equation. Examples include the DOMINO solver that is a part of EDF's COCAGNE code (Moustafa et al., 2015), PARTISN code developed at LANL (NEA, 2009) and the Denovo S_N module in the SCALE code (developed at ORNL) (Evans et al., 2010). Therefore, error estimation for this spatial discretisation is of interest to the nuclear industry.

It is often not the error in the neutron flux solution that is of interest to the nuclear engineer, but the error in an engineering quantity of interest (QoI) that is a functional of the flux. Examples may include a neutron detector response or the neutron absorption in a particular reactor component. Error estimates for

these QoI are called goal-based error estimates. The aim of this paper is to derive an estimate for the error introduced in a QoI due to the DD spatial discretisation of the multi-dimensional transport equation. Only cartesian geometries are considered due to the cartesian nature of the DD method.

Goal-based error estimation and adaptive mesh refinement (AMR) are well-known techniques used in the finite element (FE) community (Bangerth and Rannacher, 2003). They estimate the discretisation error in a QoI that is a functional of the solution to a partial differential equation (PDE). These methods involve directly calculating a dual weighted residual (DWR) (Lathouwers, 2011a,b) or replacing this inner product by norms of estimations to the errors in the forward and dual solutions (Wang and Ragusa, 2011). Due to the prevalence of other discretisation schemes that are not generally considered as FE schemes, research has also been conducted to find equivalent methods for other differencing schemes (Fidkowski and Darmofal, 2011; Pierce and Giles, 2000; Giles et al., 2004; Chen and Gunzburger, 2014; Venditti and Darmofal, 2002).

Error estimation methods (for arbitrary functionals) have been applied to FE discretisations of the neutron transport equations (Wang and Ragusa, 2011; Lathouwers, 2011a,b). DWR methods were used to derive an estimate of the L^2 error in nodal methods but properties associated with this particular goal value (and assumptions on the regularity of the solutions) were used to replace the adjoint solution by bounds to the adjoint solution given in terms of the solution to the forward (or primal) problem (Duo et al., 2009). This method removes the need to solve a dual problem, but does not allow for estimating the error in arbitrary goal functionals. Goal-based error estimation and AMR have been applied to the 1-D DD-S_N equations by using the fact that the equations are equivalent to a weighted residual scheme (Pitkäranta, 1978; Jeffers et al., 2017). This view by definition gives a functional definition of the flux variation in space. This allows for the calculation of a residual and the ability to weight the resulting function with an adjoint function calculated using the same method (Jeffers et al., 2017). In other differencing schemes that are not derived by assuming that the solution resides in a given space, means that one needs to map calculated unknowns into a solution space (Giles et al., 2004). Another option is to derive a discretised equivalent to the weighted residual scheme (Venditti and Darmofal, 2002). The latter is not advisable in the DD case due to the fact that the discretisation is not adjoint consistent (see (Jeffers et al., 2017; Jeffers, 2017)).

The DD method is the traditional way of extending the 1-D DD equations to 2-D (Lewis and Miller, 1993) and is the method employed in multi-dimensional DD-S_N neutron transport codes. This view of the DD-S_N method was later extended to higher orders for single and multi-dimensional problems (Hébert, 2006; Martin and Hébert, 2009). However, the box method is what is obtained if the WR view of the 1-D method (presented in (Jeffers et al., 2017)) is extended to 2-D. It is referred to as the box method in this paper since this is the name given to it in previous literature (Valougeorgis, 1988). We show an equivalence between the box method and the traditional DD method.

We also show that the box method can be extended to higher orders. An equivalence between Hébert high order DD method (Hébert, 2006; Martin and Hébert, 2009) and the higher order box method is also shown in this paper. However, it is important to note that more information is kept about the point-wise approximation of the solution in the latter case. We explain the equivalence by first showing the equivalence in 1-D between Hennart's WR view of the DD equations and Hébert view. This equivalence can then be extended to 2-D between the higher order box methods and the higher order Hébert methods.

Methods for obtaining a DWR error estimation for both schemes are suggested and applied to the box method and traditional DD method for a variety of 2-D fixed (extraneous) source and K_{eff} eigenvalue cases. Although AMR has been applied to the DD scheme in the past (Aussourd, 2003; Baker, 2002) the refinement was not driven by goal-based error indicators. DWR driven AMR has previously been applied to the DD scheme in 1-D (Jeffers et al., 2017) but multi-dimensions would bring in new challenges which are discussed at the end of this paper.

The paper is organised as follows. Section 2.1 describes the traditional 2-D DD-S_N discretisation. The lowest order box method, previously used by (Valougeorgis, 1988) is obtained in section 2.2 by extending the WR view of the 1-D DD-S_N equations to 2-D. An equivalence is found between the box and traditional DD methods in section 2.3. Various practical conclusions can be drawn from this equivalence and are discussed in section 2.4. An explanation of how the box method can be extended to higher orders is given in section 3.1. The equivalence between the Hennart and Hébert views of the higher order DD-S_N equations in 1-D is explained in section 3.2.1. This explanation is then extended to multi-dimensions in section 3.2.2. The DWR theory applied to the box and traditional DD methods is explained in section 4. The results given by applying DWR error estimation to the lowest order box and DD methods are given in section 5. An

explanation as to why DWR driven AMR has not been applied to multi-dimensional problems as was done for the 1-D case is given in section 6. A discussion of a possible extension to 3-D problems is given in section 7. The conclusions of the paper are given in section 8.

2. The DD and box method in multi-dimensions

This section presents the DD and the box-methods applied to the already angularly discretised (S_N) neutron transport equation. Note that isotropic scattering is always assumed in this paper since these methods are better adapted for more diffusive schemes. This is because anisotropic scattering can generate negativities in the angular source, which can then lead to negative angular fluxes. When this occurs in DD schemes people often use negative flux fix-up, and in this case, the mathematical structure of the DD scheme changes.

2.1. The traditional 2-D DD-S_N method

For a given angular direction of the S_N scheme, with components μ_m and η_m in the x and y direction respectively, the 2-D diamond difference equations are as follows:

$$\mu_m \frac{\bar{\Phi}_{i+\frac{1}{2},j,m} - \bar{\Phi}_{i-\frac{1}{2},j,m}}{\Delta x_{i,j}} + \eta_m \frac{\bar{\Phi}_{i,j+\frac{1}{2},m} - \bar{\Phi}_{i,j-\frac{1}{2},m}}{\Delta y_{i,j}} + \Sigma_t \bar{\Phi}_{i,j,m} = \frac{\Sigma_{s0}}{4\pi} \sum_{m=1}^{\frac{N(N+2)}{2}} \pi w_m \bar{\Phi}_{i,j,m} + \bar{Q}_{i,j,m}, \quad (1)$$

$$\bar{\Phi}_{i,j,m} = \frac{\bar{\Phi}_{i+\frac{1}{2},j,m} + \bar{\Phi}_{i-\frac{1}{2},j,m}}{2}, \quad (2)$$

$$\bar{\Phi}_{i,j,m} = \frac{\bar{\Phi}_{i,j+\frac{1}{2},m} + \bar{\Phi}_{i,j-\frac{1}{2},m}}{2}, \quad (3)$$

where the flux terms are defined as follows:

$$\bar{\Phi}_{i,j,m} = \frac{1}{\Delta x_{i,j} \Delta y_{i,j}} \int_{x_{i-\frac{1}{2}}}^{x_{i+\frac{1}{2}}} \int_{y_{i-\frac{1}{2}}}^{y_{i+\frac{1}{2}}} \Phi_m(x,y) dx dy, \quad (4)$$

$$\bar{\Phi}_{i\pm\frac{1}{2},j,m} = \frac{1}{\Delta y_{i,j}} \int_{y_{i-\frac{1}{2}}}^{y_{i+\frac{1}{2}}} \Phi_m(x_{i\pm\frac{1}{2}},y) dy, \quad (5)$$

$$\bar{\Phi}_{i,j\pm\frac{1}{2},m} = \frac{1}{\Delta x_{i,j}} \int_{x_{i-\frac{1}{2}}}^{x_{i+\frac{1}{2}}} \Phi_m(x,y_{j\pm\frac{1}{2}}) dx. \quad (6)$$

Subscripts i and j correspond to the ith cell in the x-direction and the jth cell in the y-direction respectively. Equations (1)-(3) are an extension of the DD-S_N equations in 1-D:

$$\mu_m \frac{\psi_{i+\frac{1}{2},m} - \psi_{i-\frac{1}{2},m}}{\Delta x_i} + \Sigma_t \bar{\psi}_{i,m} = \frac{\Sigma_{s0}}{2} \sum_{m=1}^{N} w_m \bar{\psi}_{i,m} + \bar{q}_{i,m}, \quad (7)$$

$$\bar{\psi}_{i,m} = \frac{\psi_{i+\frac{1}{2},m} + \psi_{i-\frac{1}{2},m}}{2}. \quad (8)$$

However, in the 1-D example, ψ represents the angular flux integrated over the azimuthal angle (hence the division by 2 instead of 4π in the isotropic scatter term in equation (7) compared to (1)). In the 1-D example, $\psi_{i+\frac{1}{2},m}$ and $\psi_{i-\frac{1}{2},m}$ represent cell-edge point values and and $\bar{\psi}_i$ the average over cell i. w_m represent angular quadrature weights that sum to 1 over all angular quadrature ordinates in the 1-D case and to 4 in the 2-D case.

2.2. 2-D box method as an extension of the 1-D WR view of the DD equations

In the lowest order 1-D DD case, the vertex values at the edges of each cell in the discretised domain are the unknowns solved for. Linear behaviour within the cell can be inferred from the DD auxiliary equation for each cell. This means that the approximate solution is "uniquely determined by its values at cell boundaries"

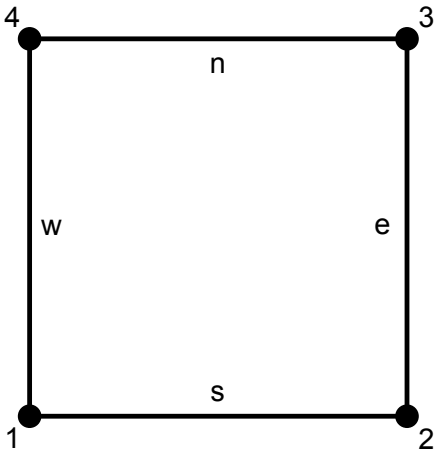

Figure 1: Node numbering for box method and DD scheme

(Pitkäranta, 1978). It has been shown that the 1-D DD scheme is equivalent to a Petrov-Galerkin finite element scheme, in that it is a WR scheme with piece-wise constant test functions and piece-wise linear trial functions (Pitkäranta, 1978; Jeffers et al., 2017). The representation of the angular flux within a given cell, for a given angle can be expressed as:

$$\Phi(x)_{\text{cell}} = \Phi(\zeta) = c_1 + c_2\zeta \tag{9}$$

where:

$$\zeta = \frac{2x - x_i - x_{i+1}}{x_{i+1} - x_i}, \tag{10}$$

The subscripts i and $i+1$ are used to indicate the left and right sides of cell i respectively.

If nc is the number of cells, then this gives nc equations for $nc+1$ parameters per angle. The remaining parameter is given by imposing an essential Dirichlet boundary condition for each angle.

Pitkäranta notes that this method can be extended in to 2-D by choosing piece-wise constant test functions and piece-wise bilinear trial functions (Pitkäranta, 1978):

$$\Phi(x,y)_{\text{cell}} = \Phi(\zeta,\gamma) = c_1 + c_2\zeta + c_3\gamma + c_4\zeta\gamma, \tag{11}$$

where:

$$\zeta = \frac{2x - x_{\text{w}} - x_{\text{e}}}{x_{\text{e}} - x_{\text{w}}}, \tag{12}$$

$$\gamma = \frac{2y - y_{\text{s}} - y_{\text{n}}}{y_{\text{n}} - y_{\text{s}}}, \tag{13}$$

and the subscripts e, w, n and s represent the east, west, north and south sides of a given cell, as shown in figure 1.

The trial space (for a given angular direction) in this case is a $(n_x+1)(n_y+1)$-dimensional space, where n_x and n_y are the number of cells in the x and y dimension respectively. Pitkäranta notes that the approximate solution is then determined uniquely by the vertex values. Weighting by each basis function of the test space gives $(n_x n_y)$ equations and $(n_y + n_x + 1)$ boundary conditions are then imposed on the trial space in a point-wise fashion in order to be able to solve for all vertex unknowns.

The solution within a cell in terms of the vertex values for a given angular direction is:

$$\Phi(x,y)_{\text{cell}} = \Phi(\zeta,\gamma) = \Phi_1 N_1(\zeta,\gamma) + \Phi_2 N_2(\zeta,\gamma) + \Phi_3 N_3(\zeta,\gamma) + \Phi_4 N_4(\zeta,\gamma), \tag{14}$$

where

$$N_1(\zeta,\gamma) = \frac{1}{4}(1-\zeta)(1-\gamma), \tag{15}$$

$$N_2(\zeta,\gamma) = \frac{1}{4}(1+\zeta)(1-\gamma), \tag{16}$$

$$N_3(\zeta,\gamma) = \frac{1}{4}(1+\zeta)(1+\gamma), \tag{17}$$

$$N_4(\zeta,\gamma) = \frac{1}{4}(1-\zeta)(1+\gamma). \tag{18}$$

Equations (15)-(18) show the local variation of N_k (where k is the vertex number as shown in figure 1) over a single cell. Each N_k is a globally continuous function in terms of x and y that is unity at the associated node and zero at all other nodes, resulting in a bilinear tent function.

The test function space is discontinuous and defined as follows:

$$M_{i,j}(x) = \begin{cases} 1 & \text{if } x \in (x_i, x_{i+1}) \text{ and } y \in (y_i, y_{i+1}) \\ 0 & \text{otherwise} \end{cases} \qquad \text{for } i = 1, 2, \ldots, n_x \text{ and } j = 1, 2, \ldots, n_y. \tag{19}$$

Keeping the vertex values as the unknown parameters gives equation (20), see figure 1 for node numberings. There are 4 vertex values in each cell, 3 of them (points 1,2 and 4 for $\mu > 0$ and $\eta > 0$) are determined by the imposed essential boundary conditions or values calculated for previous cells in the sweep. These values are assumed continuous between cells by searching for a function in a subspace of H^1 for each ordinate. The remaining unknown (point 3 for $\mu > 0$ and $\eta > 0$) can then be calculated from the equation that results from the WR procedure. The equations that result are the same as the *box method* used by Valougeorgis (Valougeorgis, 1988):

$$\frac{\mu}{2\Delta x_{ij}}\left(\Phi_3 + \Phi_2 - \Phi_4 - \Phi_1\right) + \frac{\eta}{2\Delta y_{ij}}\left(\Phi_3 + \Phi_4 - \Phi_1 - \Phi_2\right) + \frac{\Sigma_{t,ij}}{4}\left(\Phi_3 + \Phi_2 + \Phi_4 + \Phi_1\right) = q_{ij}. \tag{20}$$

However, in Pitkäranta's derivation of the WR DD method, vertex terms are collected together in the resulting equations (Pitkäranta, 1978, eq.34) to form the traditional 2-D DD equations (see (1)-(3)). The implications of this step is discussed in section 2.3.

The WR method is extended to multi-ordinate problems in exactly the same way as in 1-D (Jeffers et al., 2017). Hence, the trial functions map out a subspace of $(H^1)^{\frac{N(N+2)}{2}}$ and the test functions map out a subspace in $(L^2)^{\frac{N(N+2)}{2}}$.

The box method seeks a *strong* solution to the neutron transport equation and not a *weak* solution. This is because (in the multi-ordinate case) a solution to the angular flux is sought in a subspace of $(H^1)^{\frac{N(N+2)}{2}}$. Less regular solutions than $(H^1)^{\frac{N(N+2)}{2}}$ will therefore not be well represented by the box method (neither by the DD method due to the equivalence that will be shown in section 2.3).

The most regular the scalar flux can be will be when it is a member of $H^{\frac{3}{2}}$ (Johnson and Pitkäranta, 1983; Wang and Ragusa, 2009). However, in pure absorber or void regions, the regularity of the solution can reduce to $H^{\frac{1}{2}}$. It is for this reason that test cases with regions such as this will not be well-represented by the box method. In PWR reactors there are very few void or purely absorptive regions and thus the box method can be deemed appropriate. However, it would not be the most appropriate solution method for other reactor designs such as boiling water reactors (BWRs) or advanced gas cooled reactors (AGRs), where there would be large void regions (Tellier and Hébert., 2008; Stacey, 2007). Similarly, it would not be the most appropriate discretisation scheme to use when modelling a loss of coolant (LOC) accident in a PWR reactor, as this would also result in the need to model void regions. Finally, shielding applications can also contain discontinuities that would render the use of a DD-S_N code unsuitable (Duo and Azmy, 2007).

One example of a test case that has a solution in $H^{\frac{1}{2}}$ is the case of a homogeneous, purely absorbing, square domain, with zero volumetric source and different incoming fluxes on the two incoming boundaries (Duo, 2008). In this case the solution is discontinuous, and thus the box method will not converge to the correct point-wise solution as the cell-size reduces.

Oscillations are still observed when the solution is in H^1, such as the vacuum boundary condition, homogeneous, pure-absorber, constant source, square domain problem. In this case the flux is continuous but the first order derivatives are discontinuous (Duo, 2008). In the box method, the basis functions for the approximation can be discontinuous in gradient at cell edges, but have continuous gradients within the cell (15)-(18). The oscillations observed are therefore due to the discontinuous gradients not being aligned with mesh cell edges, where the slope is allowed to vary discontinuously in the approximate solution.

2.3. The equivalence of the box method and the traditional 2-D DD method

In Pitkäranta's paper, the point values of equation (20) are collected together to give an equation in terms of averaged cell and cell-edge values as in the traditional formulation of the 2-D DD equations. How to reconstruct the point-wise approximation from these values is not explained.

Once terms in the WR equation for the cell have been collected into averaged face values (21), there are still 4 unknowns for the cell. It is now only possible to define 2 boundary terms and there remain 2 unknowns:

$$\frac{\mu}{\Delta x_{ij}}\left(\bar{\Phi}_e - \bar{\Phi}_w\right) + \frac{\eta}{\Delta y_{ij}}\left(\bar{\Phi}_n - \bar{\Phi}_s\right) + \frac{\Sigma_{t,ij}}{4}\left(\bar{\Phi}_e + \bar{\Phi}_w + \bar{\Phi}_n + \bar{\Phi}_s\right) = q_{ij}. \tag{21}$$

Both remaining unknowns cannot be solved for using the single WR equation for the cell. The diamond difference auxiliary equations must be used instead:

$$\bar{\Phi}_c = \frac{\bar{\Phi}_e + \bar{\Phi}_w}{2}, \tag{22}$$

$$\bar{\Phi}_c = \frac{\bar{\Phi}_n + \bar{\Phi}_s}{2}. \tag{23}$$

Equations (22) and (23) are consistent with a bilinear functional representation within the cell, but it must be noted that in taking this approach the ability to reconstruct the bilinear term from the unknowns solved for is lost.

If the vertex values have been solved for using the box method, it is possible to calculate the cell averaged fluxes using the following matrix multiplication:

$$\begin{bmatrix} \bar{\Phi}_s \\ \bar{\Phi}_n \\ \bar{\Phi}_e \\ \bar{\Phi}_w \end{bmatrix} = \mathcal{T} \begin{bmatrix} \Phi_1 \\ \Phi_2 \\ \Phi_3 \\ \Phi_4 \end{bmatrix} = \frac{1}{2} \begin{bmatrix} 1 & 1 & 0 & 0 \\ 0 & 0 & 1 & 1 \\ 0 & 1 & 1 & 0 \\ 1 & 0 & 0 & 1 \end{bmatrix} \begin{bmatrix} \Phi_1 \\ \Phi_2 \\ \Phi_3 \\ \Phi_4 \end{bmatrix}. \tag{24}$$

The transformation matrix from cell vertex values to cell edge-averaged values in (24) is denoted by $\mathcal{T}$. The determinant of $\mathcal{T}$ is zero and so $\mathcal{T}^{-1}$ does not exist. Hence it is not possible to calculate the DD approximation and recover the bilinear behaviour of the approximate solution within the cell and coefficient c_4 of equation (11) is undetermined. It could be set to an infinite number of possibilities. If a point-wise essential boundary condition was imposed instead of a weakly imposed one and the result assumed continuous (as in Pitkäranta's paper (Pitkäranta, 1978)), then these values could be inputted into the vector in equation (24), thereby determining the nodal values for that cell. To obtain these values for each cell would mean applying the same mapping to each cell by sweeping through the mesh once again. This would lead to the same piece-wise bilinear point-wise representation as the box method.

If one were to alternatively loosen the continuity condition of the DD method and arbitrarily set the bilinear term to zero within a cell, an alternative point-wise reconstruction of the flux would be possible. The DD scheme could then be viewed as a scheme that weakly imposes the boundary conditions and interface conditions and allows for a discontinuous representation of the flux (a member of $(L^2)^{\frac{N(N+2)}{2}}$).

For the rest of this paper, the globally discontinuous, piece-wise linear view, where the bilinear term is fixed to zero, will from now on be referred to as the DD method. The globally continuous, piece-wise bi-linear view will be referred to as the box method.

2.4. Practical conclusions that can be drawn from the equivalence between the box and DD methods

The previous section showed that the average and linear components of both representations to be equivalent, but the bilinear term is undetermined in the traditional DD method.

It is well-known that the DD method suffers from instabilities in 1-D when the cell size is not small enough (Lewis and Miller, 1993; Reed, 1971). It is also never guaranteed that the cell-average fluxes in 2-D shall converge to the analytical solution (Duo and Azmy, 2007; Duo, 2008). It was shown by Duo and Azmy that convergence of the cell-average fluxes was not obtained using the DD method for a homogeneous, non-scattering domain with different incoming boundary conditions (Duo and Azmy, 2007; Duo, 2008) since the analytical solution is discontinuous along the singular characteristic. In the case of equal incoming boundary sources, the analytical solution is continuous but the gradient is discontinuous. Although the method does converge in the average cell flux value for this case, the asymptotic convergence rate is only fractional (Larsen, 1981; Duo and Azmy, 2007; Duo, 2008).

Given that the box method is a WR method it is easier to view the mathematical arguments for the convergence of the box method. It is also clear that any instabilities that result will also be shown in the DD method thanks to the equivalence shown in section 2.3.

It was noted in section 2.2 that the box method seeks a strong solution (as opposed to a weak or classical solution) to the transport equation and thus the solution must be a member of H^1 for the WR integral to be bounded. The solution is sought in a subset of H^1 that is infinitely continuous within a cell and discontinuous in gradient at cell edges. It is for this reason that it is impossible to represent a discontinuous solution to the transport equation (such as the discontinuous benchmark used by Duo and Azmy (Duo and Azmy, 2007)) using the box method (and therefore the DD method). It is also the reason why oscillations and slow convergence are observed when the gradient discontinuity does not coincide with cell edges (such as Larsen's benchmark (Larsen, 1981)).

The above also explains why the diamond difference singular characteristic tracking (DD-SCT) algorithm, devised by Duo et al. (Duo and Azmy, 2009; Duo, 2008), has a significantly improved convergence rate compared to the traditional DD scheme for the L^2, L^1 and L^∞ error norms for Larsen's benchmark problem (Duo and Azmy, 2009; Duo, 2008). In the discontinuous test cases (Duo, 2008), the L^2 and L^1 norm error convergence rates are significantly improved when the DD-SCT algorithm is used. The L^∞ error norm, which did not converge for the DD scheme, converges at a rate close to unity for the DD-SCT scheme (Duo and Azmy, 2009). The DD-SCT method works by applying a step characteristic in the cells traversed by the discontinuity (in the result itself or its gradient) and the standard DD scheme in all other cells (Duo and Azmy, 2009; Duo, 2008).

In addition to the explanation about stability that comes from the mathematical representation of the box method and its cell-average equivalence to the DD method, a comment can be made on the implementation of accelerations schemes. EDF R&D had already developed an SP_N solver that was in a mature state of development when it was decided to develop the DOMINO S_N code. DD was chosen as the spatial discretisation scheme because of the already published results on the compatibility of using a "Raviat-Thomas discretisation of the P_1 spherical harmonic equations with Gauss-Legendre integration of the mass matrices" for use in synthetic acceleration of the source iteration scheme (Hébert, 2010). The fact that the box method gives the same cell and edge-averaged flux results means that the same arguments hold when applying the correction term to the flux in the diffusion synthetic acceleration scheme (DSA). Hence, if the box method is found to give a better approximation to the error than the DD method, the unknowns solved for can be changed without changing the acceleration scheme being used.

3. Extension to higher orders

The DD method has already been extended to higher orders by Hébert et al. (Hébert, 2006). This section shows how the box method can be extended to higher orders and the equivalence between the higher order box method and the higher order DD method.

3.1. Extending the box method to higher orders

Another way of viewing the box method is as a WR method where the trial functions are given by a first order Lagrange (Hughes, 2000) interpolation within a cell and the weighting functions are zeroth order Legendre polynomials. The ability to rearrange the coefficients of an Mth order Lagrange polynomial to give

an Mth order Legendre polynomial is what made analytical integration possible for the calculation of the DWR error estimates.

An obvious way to extend the box method to higher orders would be to use higher order Lagrange polynomials for the trial functions and higher order Legendre polynomials for the weighting functions. The approximation would be assumed continuous at all orders, as in the higher order 1-D DD methods described by Hennart (Hennart and del Valle, 1995).

In 2-D, an Mth order Lagrange polynomial used as trial functions would be associated with test functions defined as the basis of a $(M-1)$th order Legendre polynomial phase space. This would result in the solution within a cell being represented uniquely by $(M+1)^2$ nodes (see figure 2 for the case where $M=2$). The solution on $(2M+1)$ nodes would be known from boundary conditions or the results given by previous cells in the sweep. The remaining M^2 unknowns would be solved for by the M^2 WR equations that result from weighting by the basis functions of a $(M-1)$th order Legendre polynomial function. The resulting flux approximation will be represented as an Mth order 2-D Lagrange polynomial which can be rearranged and expressed as an Mth order 2-D Legendre polynomial.

3.2. The equivalence between the higher order box method and Hébert's higher order DD methods

Firstly, the 1-D Hennart/WR interpretation of the arbitrary order DD method will be compared to Hébert's interpretation of the DD formulation. In section 3.2.1, we will explain how the Mth order Hébert scheme is equivalent to the $M+1$th order Hennart scheme but with the highest order spatial moment being ignored at the output. The same idea will be extended to multi-dimensions in section 3.2.2.

3.2.1. The equivalence between Hennart and Hébert's interpretation of the higher order DD formulations in 1-D

The flux within the cell, i, is represented in terms of Hennart's trial functions as follows (equations 2.6-2.7 in (Hennart and del Valle, 1995) are repeated here):

$$\psi(\zeta)_i = \psi_l f_l(\zeta) + \psi_r f_r(\zeta) + \sum_{k=0}^{M-2} \psi_c^k f_c^k(\zeta) \tag{25}$$

where:

$$f_l = \frac{1}{2}(-1)^{M-1}\left[P_{M-1}(\zeta) - P_M(\zeta)\right], \tag{26}$$

$$f_r = \frac{1}{2}\left[P_{M-1}(\zeta) + P_M(\zeta)\right], \tag{27}$$

$$f_c^k = P_k(\zeta) - P_{M-2+m(k)}(\zeta), \tag{28}$$

and $m(k)$ is a function that takes a value of either 1 or 2 such that $M-2+m(k)$ and k have the same parity. ζ is defined in terms of x for a given cell as in equation (10) and so varies as [-1,+1] along a given cell. $P_k(\zeta)$ are Legendre Polynomials such that:

$$\int_{-1}^{+1} P_k(\zeta)P_l(\zeta)d\zeta = \delta_{kl}N_k, \tag{29}$$

$$\int_{x_i}^{x_{i+1}} P_k\left(\frac{2x-x_i-x_{i+1}}{\Delta x_i}\right) P_l\left(\frac{2x-x_i-x_{i+1}}{\Delta x_i}\right) dx = \frac{\Delta x_i}{2}\int_{-1}^{+1} P_k(\zeta)P_l(\zeta)d\zeta \qquad = \delta_{kl}N_k\frac{\Delta x_i}{2}, \tag{30}$$

where:

$$N_k = \frac{2}{2k+1} \tag{31}$$

and δ_{kl} is the Kronecker delta function.

Continuity of the trial functions between the cells gives the value of ψ_l (ψ_r) when $\mu > 0$ ($\mu < 0$). The remaining $M-1$ unknowns are solved for using a WR method. The weighting functions (also called test functions) are the $M-1$ Legendre polynomials that are defined as non-zero only within the cell.

It is clear that the function within a cell can be rearranged to give:

$$\psi(\zeta)_i = \sum_{k=0}^{M} \psi_c^k P_k(\zeta), \quad \text{for M=1,2,}\ldots. \tag{32}$$

which will be useful for comparison with Hébert's scheme later in the section. In Hennart's representation, it is the M=1 scheme that is equivalent to the traditional DD scheme.

Hébert explained in his 2006 article (Hébert, 2006) that the flux is expanded in terms of a Legendre polynomial basis in each cell:

$$\psi(u)_i = \sum_{k=0}^{M} \tilde{P}_k(u)\psi_{c,i}^k, \quad \text{for M=0,1,}\ldots. \tag{33}$$

and that $M = 0$ corresponds to the traditional DD equations. $\tilde{P}_k(u)$ are the normalised Legendre Polynomials where u varies from -0.5 to $+0.5$ as follows:

$$u = \frac{2x - x_i - x_{i+1}}{2\Delta x_i}. \tag{34}$$

The Legendre Polynomials used in Hébert's derivation are normalised differently such that the equivalent of equation (30) for the normalised Legendre Polynomials is:

$$\int_{x_i}^{x_{i+1}} \tilde{P}_k\left(\frac{2x - x_i - x_{i+1}}{2\Delta x_i}\right)\tilde{P}_l\left(\frac{2x - x_i - x_{i+1}}{2\Delta x_i}\right)dx = \Delta x_i \int_{-0.5}^{+0.5} \tilde{P}_k(u)\tilde{P}_l(u)du = \delta_{kl}\Delta x_i, \tag{35}$$

Thus the following equality should be kept in mind when finding the equivalence between the two schemes:

$$\tilde{P}_k(u) = \sqrt{\frac{2}{N_k}}P_k(2u). \tag{36}$$

In Hébert's scheme, a set of WR equations are derived by weighting the residual by the normalised Legendre polynomial moments. Equations (19)-(21) in Hébert's paper (Hébert, 2006) are repeated in equations (37)-(39) below (but using this paper's node numbering and notation):

$$\frac{\mu}{\Delta x_i}(\psi_{i+1} - \psi_i) + \Sigma_{t,i}\psi_{c,i}^0 = Q_{c,i}^0 \quad M = 0 \text{ WR equation}, \tag{37}$$

$$\sqrt{3}\frac{\mu}{\Delta x_i}(\psi_{i+1} + \psi_i - 2\psi_{c,i}^0) + \Sigma_{t,i}\psi_{c,i}^1 = Q_{c,i}^1 \quad M = 1 \text{ WR equation}, \tag{38}$$

$$\sqrt{5}\frac{\mu}{\Delta x_i}(\psi_{i+1} - \psi_i - 2\sqrt{3}\psi_{c,i}^1) + \Sigma_{t,i}\psi_{c,i}^2 = Q_{c,i}^2 \quad M = 2 \text{ WR equation}. \tag{39}$$

It is noted that equations (37)-(39) have not yet been substituted in for the *approximate flux solution* (33). Hébert then proceeds to find auxiliary equations to close the system by writing the the outgoing edge's flux in terms of the incoming edge's flux and the cell central moments "in such a way to cancel the $M + 1$-order term" (Hébert, 2006):

$$\psi_{i+1} + \psi_i - 2\psi_{c,i}^0 = 0 \quad M = 0 \text{ auxiliary equation}, \tag{40}$$

$$\psi_{i+1} - \psi_i - 2\sqrt{3}\psi_{c,i}^1 = 0 \quad M = 1 \text{ auxiliary equation}, \tag{41}$$

$$\psi_{i+1} + \psi_i - 2\psi_{c,i}^0 - 2\sqrt{5}\psi_{c,i}^2 = 0 \quad M = 2 \text{ auxiliary equation}. \tag{42}$$

It is the $M+1$th order term of the *gradient* of the flux that is made equal to zero. The Mth order term of the gradient of the flux is non-zero and thus the $M + 1$th order term in the flux must also be non-zero. Hébert explains that $M = 0$ corresponds to the traditional DD equations. The 0th order WR equation provides the traditional DD integral equation and ensuring the $M + 1$th order term of the gradient of the flux is equal to zero gives the traditional DD auxiliary equation. Therefore, Hébert's DD0 method does have a non-zero first order Legendre polynomial term (with all higher order terms equal to zero) and thus the representation of the flux given by equation (33) (and equation 16 of Hébert's paper) does not represent the assumptions made of the solution in the derivation of the numerical scheme.

The representation of the flux given by equation (33) could lead one to think that the $M+1$th order flux and source terms are zero. If this were the case, substituting in for these terms in the $M+1$th WR equation then provides the auxiliary equations. However, this would lead to a mathematical inconsistency, and is therefore not the case. This can be easily demonstrated in the lowest order (traditional DD) case. If all flux spatial moments of order > 0 were equal to zero, the right and left flux values would be the same by definition. Equation (37) would then be reduced to a simple relation between that which is produced and consumed within the cell (with no streaming term). It also means that the solution of equation (38) is trivial. The only way ψ_i, ψ_{i+1} and $\psi^0_{c,i}$ can be different from each other is if the flux variation within the cell is of a higher order than zero. The WR equation used in (37) is the same as Hennart's scheme and the auxiliary equation (40) is obtained by enforcing a linear variation in the cell (setting the first order component of the flux gradient to zero). This means that Hébert's method is equivalent to Hennart's method. Hébert's scheme is therefore equivalent to a WR scheme that has trial and test functions from different spaces. However, in the representation of the flux in equation (33) Hébert does not calculate the (non-zero) $M+1$ term assumed by the method. To reduce confusion, Hébert's "Mth" order scheme refers to the number (M) of test functions (WR equations) in the scheme, whereas Hennart's "Mth" order scheme refers to the number of non-zero coefficients when the function within a cell is represented as a sum of Legendre polynomials (with no ignored terms). Thus, Hébert's Mth order scheme is equivalent to Hennart's $M+1$th order scheme, and Hébert ignores the $M+1$th term in the final representation of the flux in (33).

This equivalence extends to higher orders once the differences in the normalisation of the Legendre polynomials are taken into account. Equation (36) means that the cell central moments provided by Hébert's scheme relate to the cell central moments provided by Hennart's scheme as follows:

$$\psi^k_{c,i,\text{Hennart}} = \sqrt{\frac{2}{N_k}}\psi^k_{c,i,\text{Hébert}} \tag{43}$$

The cell node values are the same in both cases. Therefore, substituting in for (43) in (37)-(39) and (40)-(42) for a given M order scheme results in the same equations as in the $M+1$ order Hennart scheme. Thus Hébert's Mth order method is equivalent to the Hennart's $M+1$th method with the $M+1$th moment ignored when reconstructing the flux in the spatial domain.

3.2.2. The equivalence of the higher order box-method and Hébert's higher order DD method in multi-dimensions

An equivalence between the box and traditional DD method has been shown in the previous section. The first 3 Legendre polynomial coefficients can be calculated from the traditional DD unknowns, but the fourth (the bilinear term) cannot.

For the higher order box and Hébert methods to be equivalent in the same way as the traditional box and DD methods, the first $M(M+2)$ Legendre polynomial coefficients of the box method (calculated by rearranging the Lagrange polynomial representation) must be equivalent to those that can be calculated from the Hébert method's unknowns. The final Legendre polynomial coefficient provided by the Mth order box method will not be able to be calculated from the Hébert method due to the unknowns being cell-centred and cell-edge spatial moments that average out this term.

The WR equations in Hébert's paper (equations (38), (39), (41) and (42) (Hébert, 2006)) are analytical before the auxiliary equations are substituted in for the higher order terms. Showing that the Mth order approximate function of the box scheme satisfies the auxiliary equations of a $M-1$th order Hébert DD scheme is sufficient to show that the first M^2 Legendre polynomial coefficients of the two schemes are equivalent. The next $2M$ Legendre polynomial coefficients can then be calculated from known cell edge and cell central spatial moments of the flux (in an analogous way to the linear in x and y terms for the lowest order DD method). The final Legendre polynomial cannot be calculated as a function of the cell centre and cell edge moments as this information is lost by taking integral values.

The above equivalence has been demonstrated for the bi-quadratic scheme in appendix D of (Jeffers, 2017). Numerical analysis of this equivalence for higher orders is beyond the scope of this paper.

A comment may be made about the practicality of calculating the DWR for the higher order box method. Rearranging the Lagrange polynomial coefficients to give the equivalent Legendre polynomial coefficients gets more cumbersome as the order of the polynomials increases. If a higher order box method was to be considered in the future, numerical integration should be considered for calculation of the DWR integrals.

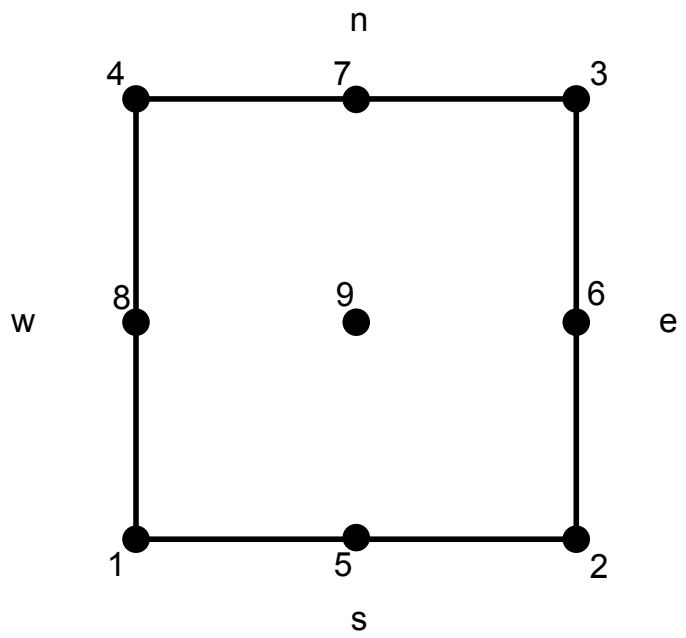

Figure 2: Bi-quadratic cell

4. DWR for box method and DD

The DWR error estimator and local indicators are easy to define for the box method due to it being equivalent to the DD method in 1-D. The form that the DWR estimator and local indicators take are given in section 4.1. In the 2-D DD case, as explained in section 4.1, one can either calculate the vertex values by taking the DD unknowns and boundary conditions and sweeping through the cells, or it can be assumed that the flux is piece-wise linear, point-wise discontinuous between cells but continuous in cell-edge fluxes. Due to these different options, different forms of the DWR estimator are given for the DD method in section 4.2.

4.1. DWR for the box method

Since the box method is the direct extension of the WR formulation of the 1-D DD equations, the DWR estimator is easily derived since it follows the exact same arguments as in 1-D:

$$\mathrm{DWR}_{\mathrm{Box}} = \sum_{i=1}^{n_x} \sum_{j=1}^{n_y} \sum_{m=1}^{\frac{N(N+2)}{2}} w_m \int_{A_{ij}} R_{\mathrm{h,Box}}(x, y, \Omega_m) \Phi_m^{\dagger}(x, y, \Omega_m) dx dy. \tag{44}$$

Where:

$$R_{\mathrm{h,Box}}(x, y, \Omega_m) = q - \mathcal{L}\Phi_{\mathrm{h,Box}}. \tag{45}$$

is continuous on cell boundaries.

The cell-wise indicators if AMR was to be conducted would then be given by:

$$\mathrm{Indicator}_{i,j} = \left| \sum_{m=1}^{\frac{N(N+2)}{2}} w_m \int_{A_{ij}} R_{\mathrm{h,Box}}(x, y, \Omega_m) \Phi_m^{\dagger}(x, y, \Omega_m) dx dy \right|. \tag{46}$$

4.2. DWR for the 2-D DD method

If the box vertex values are reconstructed in such a way as to take into account point-wise enforced boundary conditions, then the same DWR error estimator as the box method can be used (44) and it would give the same results.

If the DD method results are mapped into a discontinuous bilinear finite element space (with the bilinear term set to zero), the DWR takes the same form as that derived by Lathouwers for the DGFEM scheme (Lathouwers, 2011a,b).

This results in the following DWR for a given cell:

$$\mathrm{DWR}_{\mathrm{cell}} = \sum_{m=1}^{\frac{N(N+2)}{2}} \left(\int_{A_{cell}} \Phi^{\dagger}_{\mathrm{int}}(x,y,\Omega_m) R_{\mathrm{h}}(x,y,\Omega_m) dA \right. \\ \left. + \int_{y_s}^{y_n} \Phi^{\dagger}_{\mathrm{int}}(x,y,\Omega_m) r_{x_{in}}(x,\Omega_m) dy + \int_{x_w}^{x_e} \Phi^{\dagger}_{\mathrm{int}}(x,y,\Omega_m) r_{y_{in}}(y,\Omega_m) dx \right), \quad (47)$$

where "int" stands for internal cell value, the subscript "in" stands for the value at the incoming boundary and:

$$R_{\mathrm{h}}(x,y,\Omega_m) = q - \mathcal{L}\Phi_h, \quad (48)$$

$$r_{x_{in}}(x,y,\Omega_m) = \mu_m \left(\Phi_h(x_{\mathrm{in}} - 0, y, \Omega_m) - \Phi_h(x_{\mathrm{in}} + 0, y, \Omega_m) \right), \quad (49)$$

$$r_{y_{in}}(x,y,\Omega_m) = \eta_m \left(\Phi_h(x, y_{\mathrm{in}} - 0, \Omega_m) - \Phi_h(x, y_{\mathrm{in}} + 0, \Omega_m) \right). \quad (50)$$

The boundary term arises from the discontinuity and the weak application of boundary conditions. Instead of integrating over a cell, the integration is done over a cell that is shifted by a very small amount ξ in the upwind direction, and the answer as $\xi \to 0$ is computed (Hennart and del Valle, 1996). If the variation within the cell is approximated via a bilinear variation within the cell and the approximation to the flux is globally continuous, the boundary terms in equation (47) go to zero.

The total error in the domain is obtained by summing the values of (47) over all cells in the domain. If AMR was to be conducted, an indicator for the cell is found by taking the absolute value of (47).

5. Results of DWR error estimation for the 2D box method and DD method

This section applies the methods described in section 4.2 to various 2-D test cases. The reference solutions for calculating the true error and effectivity indices were provided by the AVARIS code (Kópházi, 2016) where analytical solutions were not available. The AVARIS reference code uses linear discontinuous finite elements for the spatial discretisation, a multi group energy discretisation and a discrete ordinate ($\mathrm{S_N}$) angular discretisation.

In order to improve the error estimate in the box method case without adding too much complication to the code, there is the option of calculating the adjoint solution on a more refined mesh than the forward solution. The more refined solution is then injected into the phase space of the less refined forward solution. This was not conducted for linear DD since how to conduct the injection into the phase space without introducing more errors is not obvious. In practice, calculating a more accurate adjoint solution may seem counter-productive if one is searching for an accurate solution to a functional of the forward flux. However, when error estimation is deemed important, this overhead could be justified. In the rest of this section *ncr* represents the ratio of the number of cells along one side of the domain for the adjoint solution compared to that used in the mesh for the forward solution.

5.1. Test case 1

This test case is an S_2, homogeneous square domain (side length 9cm) with vacuum boundary conditions on all sides and unit source throughout. $\Sigma_{\mathrm{t}} = 1.0\mathrm{cm}^{-1}$. Many different scatter ratios $\left(c = \frac{\Sigma_{\mathrm{s0}}}{\Sigma_{\mathrm{t}}}\right)$ are tested: $c = 0.0, 0.1, 0.5, 0.7, 0.9, 0.99$.

When $c = 0$, the analytical solution to the flux can be calculated as described in Duo's thesis (Duo, 2008). Reference results for higher values of c were provided via the AVARIS code (Kópházi, 2016), using a highly refined DGFEM mesh and the same angular quadrature.

For $c \geq 0.1$, two goal quantities are tested: the integral of the scalar flux throughout the domain (denoted by Test case *a* - which is also applied to the case where $c = 0$) and the integral throughout a quarter slice of the domain (denoted by Test case *b*).

This collection of test cases was used to provide a set of simple test cases for debugging, but also to show the effects of varying scatter ratios on the accuracy of the DWR error estimators for different goal quantities.

5.1.1. Test case 1a

Figure 3a gives the effectivity index (the ratio of the magnitude of the error estimator to the magnitude of the true error in the QoI) of the 4 different DWR estimators at the 6th mesh iteration. Figure 3b is the same but with the DD plot removed for clarity. Figure 4 plots the convergence graphs of the true error and all error estimators. The true error resulting from the box method code and DD code are plotted and are exactly the same due to the equivalence between the two methods for integral quantities.

Figure 3a shows that all error estimators give an effectivity index near unity for high values of c. The estimator given by the DD method described in section 4.2 gives the worst result for low values of c. Figure 4 shows that, for low values of c, the effectivity index given by the DD DWR gets worse as the mesh becomes more refined. This is due to the convergence plot of the DWR error estimate in the DD case having a different slope from that of the reference error. The exception is when $c = 0.99$ (figure 4f), where the DD estimator tends to the correct slope and value.

Figure 3b shows that the effectivity index tends to unity as c is increased for all box method error estimators. The effectivity indices at low c, although all far from unity, are more correct when the error estimator uses a more accurate adjoint solution. The effectivity index reduces from 47 when $ncr = 1$ to 18 when $ncr = 2$, then reducing further to 15 when $ncr = 3$. The increase in the accuracy of the error estimate with an increased value of ncr is limited given that the more accurate result is mapped into the same space as the forward mesh for simplicity. Thus, although an accurate solution to the adjoint solution may be found on a highly refined mesh, some error is re-introduced by mapping it into the low order space.

All box method DWR estimators have the same slope as the true error in figure 4, with the exception of $c = 0.5$ (for all mesh iterations) and $c = 0.7$ (for the first few mesh iterations). This suggests that the reason for the DD DWR estimator's incorrect slope is due to the bilinear term being artificially set to zero. The box method representation conserves the bilinear term resulting in a more accurate error estimate.

The box method DWR estimator (which conserves the bilinear term), although having the correct slope, does not coincide with the graph of the true error at low values of c. The approximation to the flux for low values of c is oscillatory due to the lack of regularity in the analytical solution. For example, when $c = 0.0$, the discontinuity in the gradient of the flux is not aligned with cell boundaries and thus the solution will be badly represented by the box/DD method. The discontinuous behaviour reduces as c increases. Thus, the oscillations observed in the approximate solution reduce in magnitude as c increases or as the number of cells in the mesh is increased. The goal QoI is an integral value, thus as long as the solution is oscillating around the correct value of the flux, cancellation of errors in integration will result in only a small contribution from solution oscillation to the final error in the integral functional. However, this is not the case for the error estimator. Oscillations are observed in both the forward and adjoint flux approximations, thus, two oscillating functions are multiplied together before being integrated in the DWR calculation. Because of this, the cancellation of errors observed in the approximation to the goal functional does not occur for the DWR estimate, thus explaining the overestimation of the error by the DWR error estimator. The improvement of the effectivity index when using a more refined mesh for the adjoint solution is mainly due to the reduction observed in the oscillations.

5.1.2. Test case 1b

All error estimators give an effectivity index close to unity (figure 5a), even the DD DWR error estimator. Though, the estimators that conserve the bilinear term still consistently perform better than the DD DWR error estimator. Figure 5b plots only the box method DWR error estimators, and it is observed that the effectivity index improves when a more accurate approximation to the adjoint solution is used. Although the effectivity index is close to unity for all values of c, an improvement is observed as c is increased. The convergence graphs in figure 6 also show how all error estimates well-represent the true error for all values of c.

This improvement compared to test case 1a is due to the lack of symmetry in the forward and adjoint flux solutions meaning that the oscillations in the solutions are not amplified by the inner product of the error estimator.

5.2. Test case 2

This is the EIRA-2A benchmark problem defined in (Stepanek et al., 1982). The geometry and cross sections are given in figure 7. Reference results for this test case were provided via the AVARIS reference

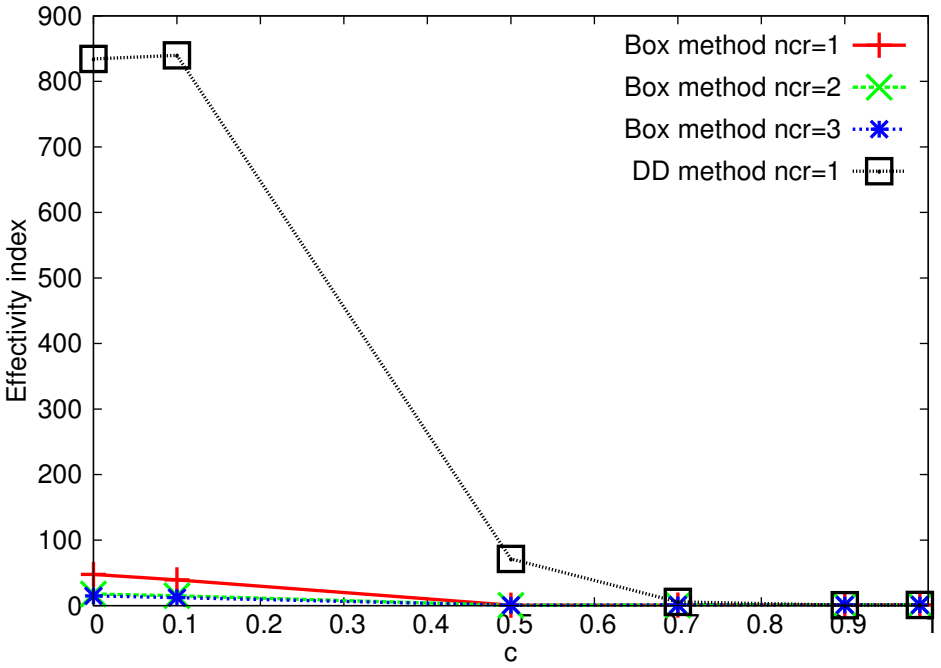

(a) Box methods and DD method

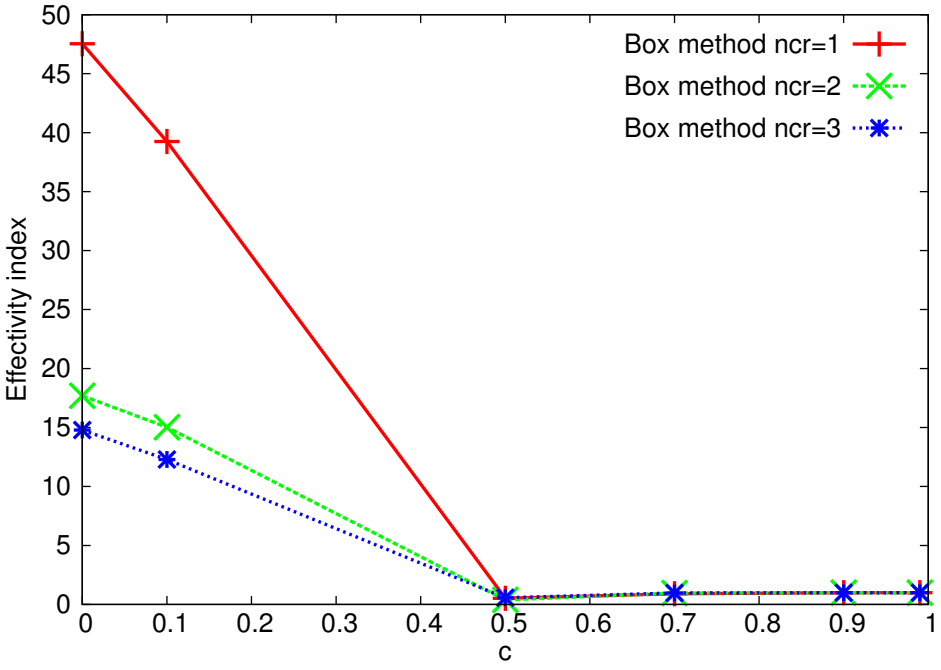

(b) Box method only

Figure 3: Test case 1a. Effectivity index as a function of the scatter ratio for a range of different error indicators at the 6th uniform mesh iteration.

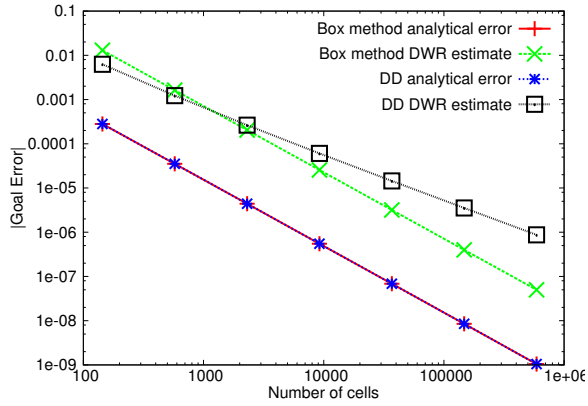

(a) c=0.0

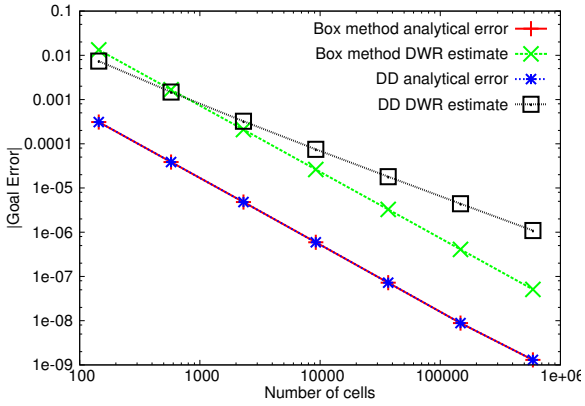

(b) c=0.1

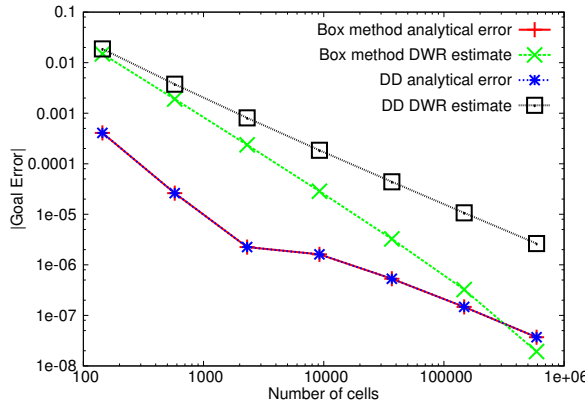

(c) c=0.5

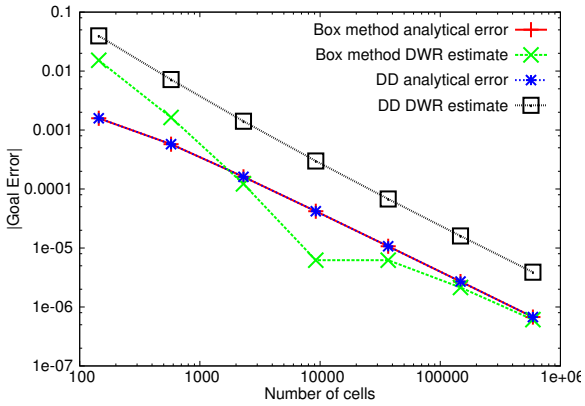

(d) c=0.7.

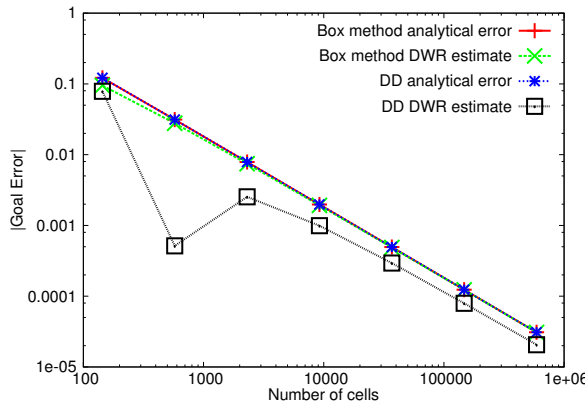

(e) c=0.9

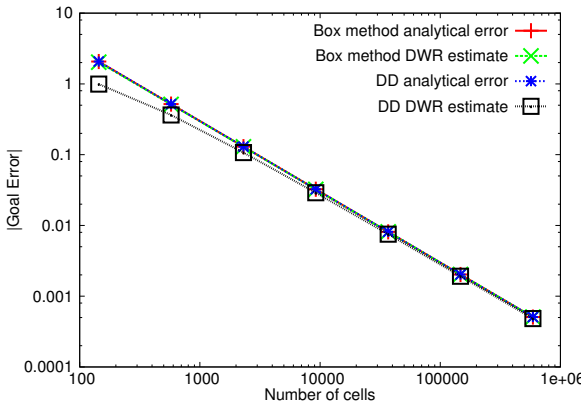

(f) c=0.99

Figure 4: Test case 1a. Convergence graphs.

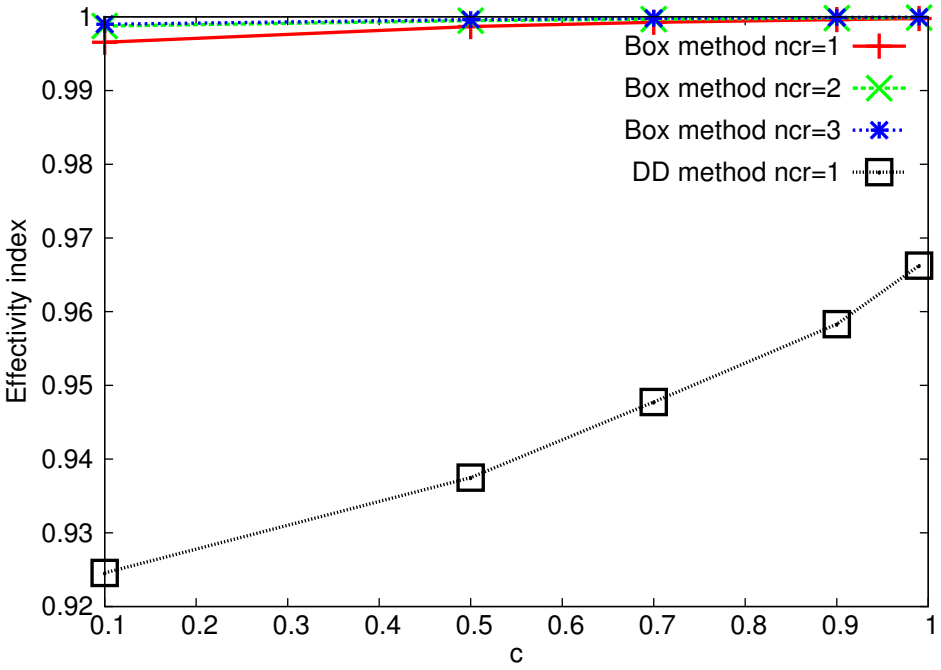

(a) Box methods and DD method.

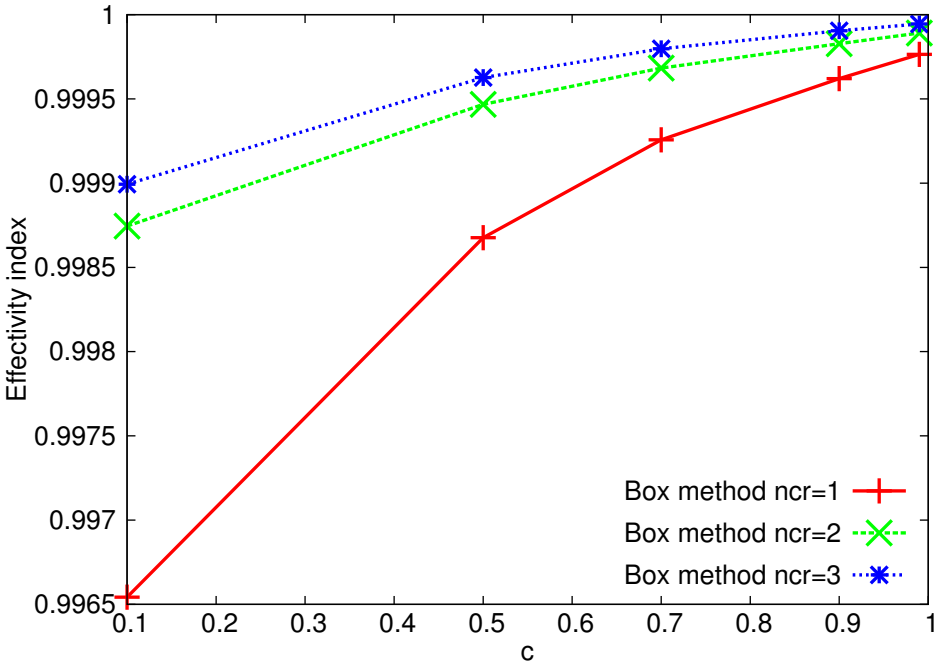

(b) Box method only.

Figure 5: Test case 1b. Effectivity index as a function of the scatter ratio for the 6th uniform mesh iteration.

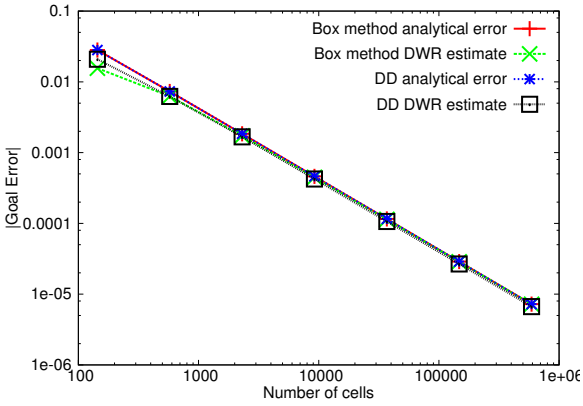

(a) c=0.1

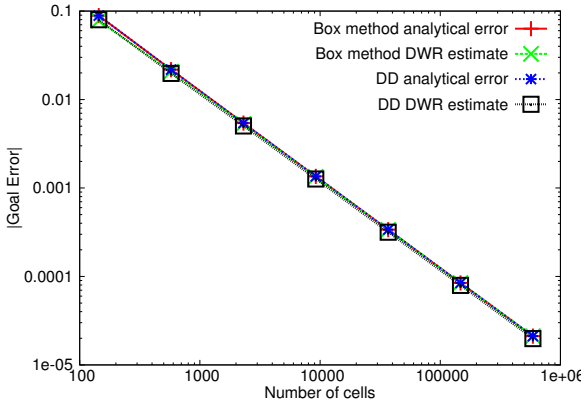

(b) c=0.5

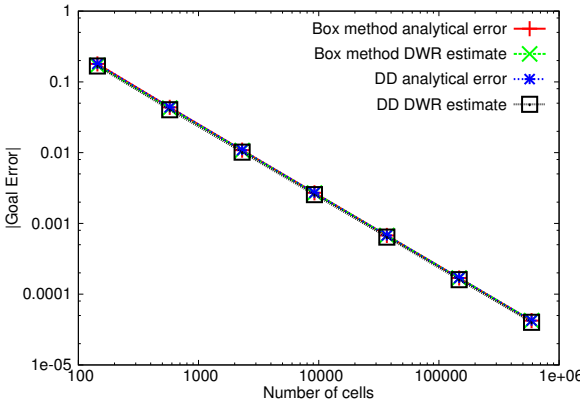

(c) c=0.7

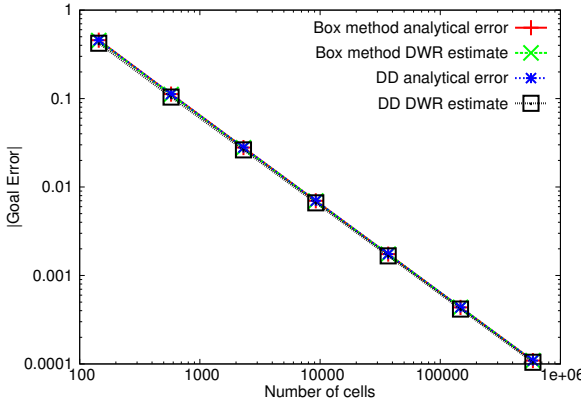

(d) c=0.9

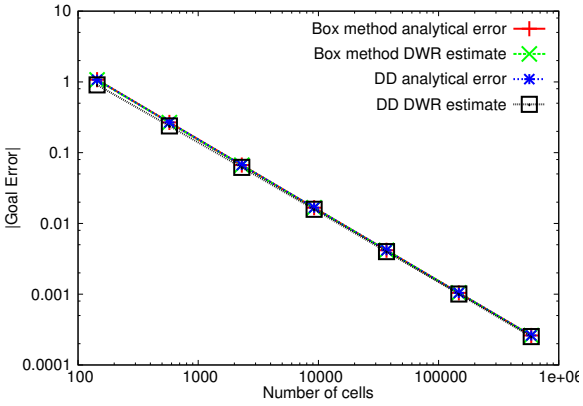

(e) c=0.99

Figure 6: Test case 1b. Convergence graphs.

code (Kópházi, 2016), using a highly refined DGFEM mesh and the same angular quadrature (S_2).

The difference between test cases 2a and 2b is the QoI. The goal QoI in test case 2a is the integral of the scalar flux throughout the whole domain. The goal QoI in test case 2b is the total absorption in the $\Sigma_t = 0.7$ box seen in figure 7.

This test case was chosen to give a more challenging heterogeneous multi-dimensional fixed source problem.

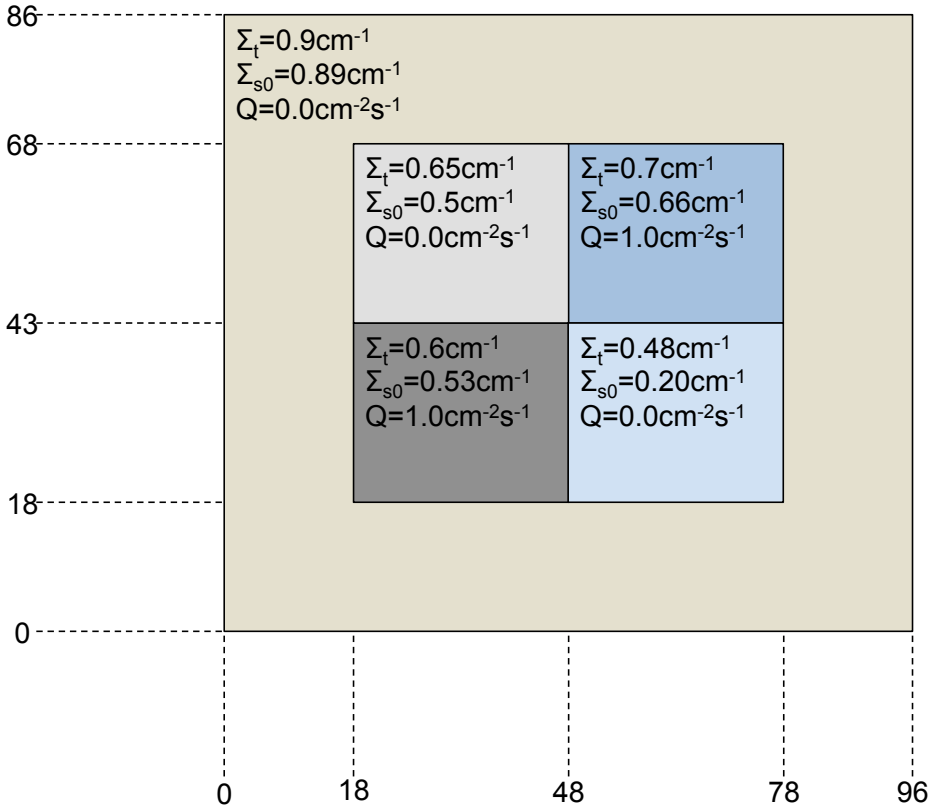

Figure 7: EIRA 2-A 2-D problem (Stepanek et al., 1982).

5.2.1. Test case 2a

The convergence plots of the error and error estimators as a function of the number of cells in the forward mesh are plotted in figure 8a. Similarly, the effectivity indices as a function of cell number are plotted in figure 8b. The effectivity index plots of only the box method DWR error estimators are re-plotted in figure 8c for clarity.

The graphs in figure 8 reinforce the conclusions drawn from the homogeneous test cases in section 5.1.1: better results are given by the box method error estimators than the DD method and the more accurate the adjoint solution, the closer the effectivity index is to unity. The divergence away from unity at the highest resolution mesh in figure 8c is due to reference solution used in the effectivity index being calculated by using a highly refined numerical solution to the forward equation and not an analytical reference. The numerical reference solution was obtained using the AVARIS code with bi-linear quadrilateral finite elements (Kópházi, 2016). Reference results were also obtained using other types of elements in the AVARIS code. The resulting variation in the effectivity index results were of the order of the deviation shown in figure 8c.

5.2.2. Test case 2b

The results for this test case are shown in figure 9. There is a big deviation between the DD error estimator and the true error (figure 9b), though the slope is correct in figure 9a. The first and second points of all box method plots in figure 9c seem to be tending towards unity before diverging again. The divergence is because

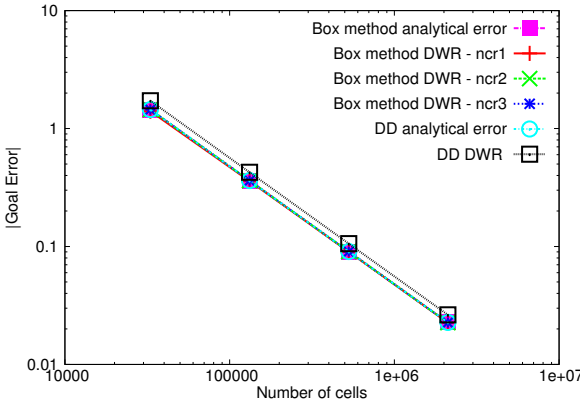

(a) Convergence

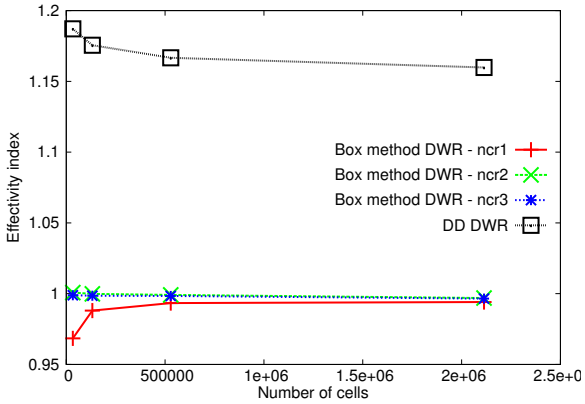

(b) Effectivity index

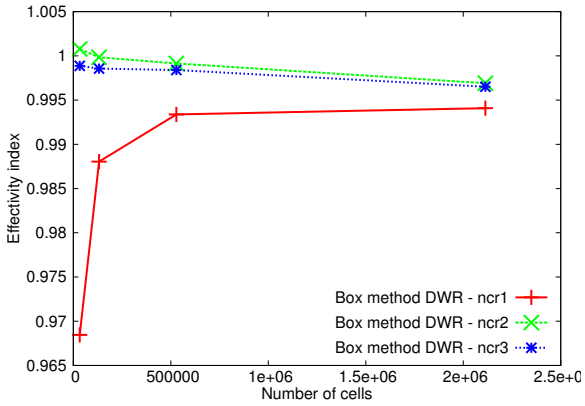

(c) Effectivity Index. Box method only.

Figure 8: Test case 2a results.

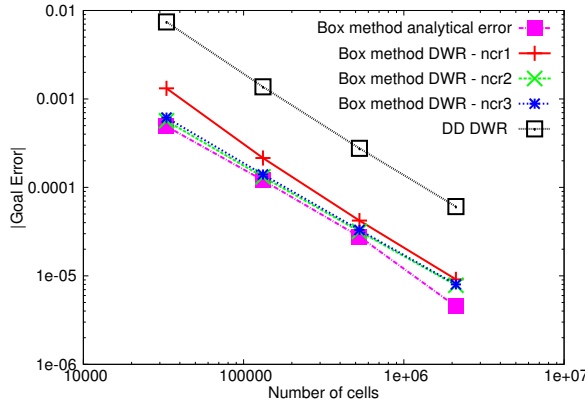

(a) Convergence

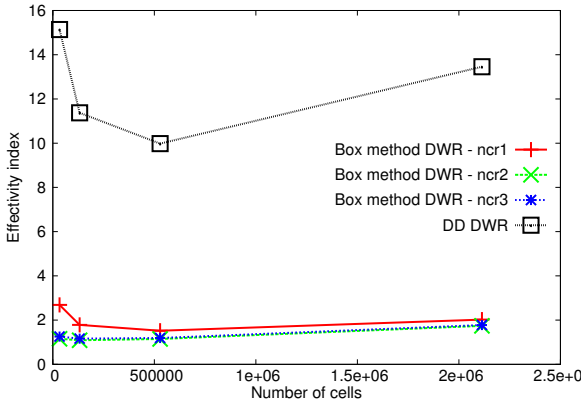

(b) Effectivity index

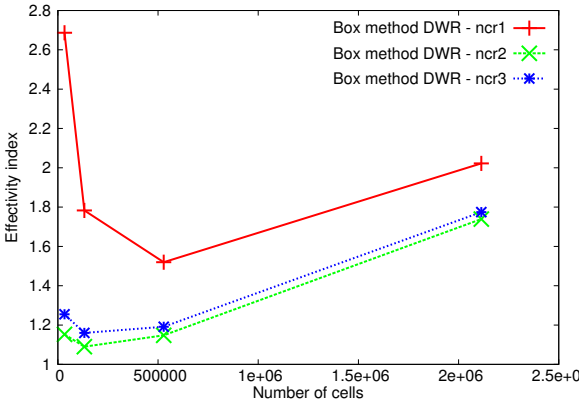

(c) Effectivity Index. Box method only.

Figure 9: Test case 2b results.

of the limited accuracy of the reference solution, the accuracy is less than for test case 2a (section 5.2.1) due to the more localised goal quantity. Increasing the accuracy of the adjoint solution results in a better error estimator. In figure 9c the effectivity index results for $ncr = 2$ are closer to one than when $ncr = 3$. This is due to the way the map into the forward mesh's space can distort the results.

5.3. Test case 3

This test case is an S_2 homogeneous square domain (5cm×5cm) with vacuum boundary conditions on all sides.

Contrary to the previous two test cases, test case 3a and 3b have the same QoI, but different values for the cross sections. Test case 3a has: $\Sigma_t = 1.0\text{cm}^{-1}$, $\Sigma_{s0} = 0.99\text{cm}^{-1}$ and $\nu\Sigma_f = 1.0\text{cm}^{-1}$. Test case 3b has: $\Sigma_t = 10.0\text{cm}^{-1}$, $\Sigma_{s0} = 9.9\text{cm}^{-1}$ and $\nu\Sigma_f = 0.2\text{cm}^{-1}$.

The QoI in these test cases is the K_{eff}. Reference results for this test case were provided via the AVARIS code (Kópházi, 2016), using a highly refined DGFEM mesh and the same angular quadrature. These test cases were chosen in order to provide simple eigenvalue test cases for debugging. This test case 3b has less leakage than 3a and should therefore be more appropriate for the DD discretisation scheme.

The results for test case 3a are shown in figure 10a. Although the slopes of all error estimators are the same as the reference error, they all significantly under-estimate the error (by a factor of the order of 50 - figure 10). This test case has a lot of leakage, and thus suffers from some of the oscillation issues that gave bad results in test case 1a (section 5.1.1). This reasoning for the underestimation is supported slightly by the small increase in the effectivity index when a more accurate adjoint solution is used for calculating DWR estimator. The large underestimation could also be due to the linearisation error not being negligible and not decreasing at the same rate as the leading order error term measured by the estimator, thus leading to a convergence to a constant effectivity index that is not unity.

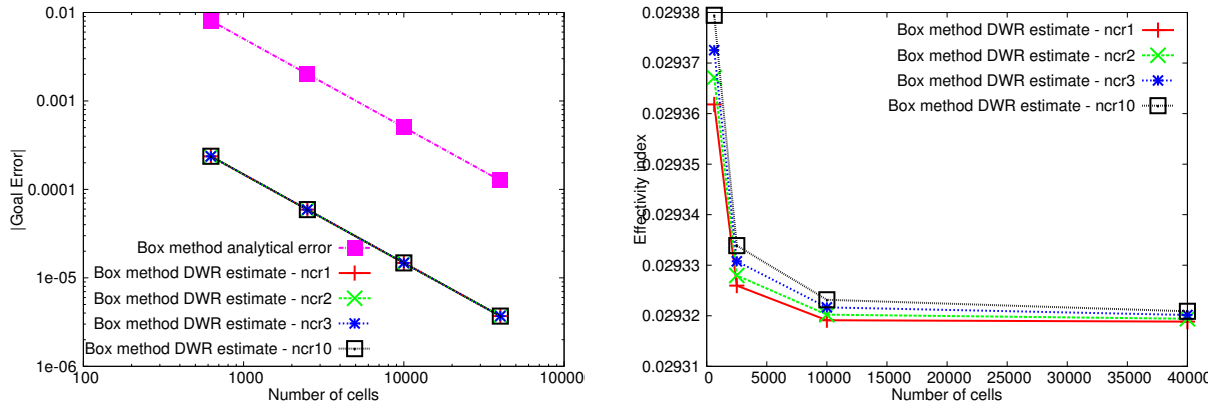

(a) Convergence (b) Effectivity index

Figure 10: Test case 3a results.

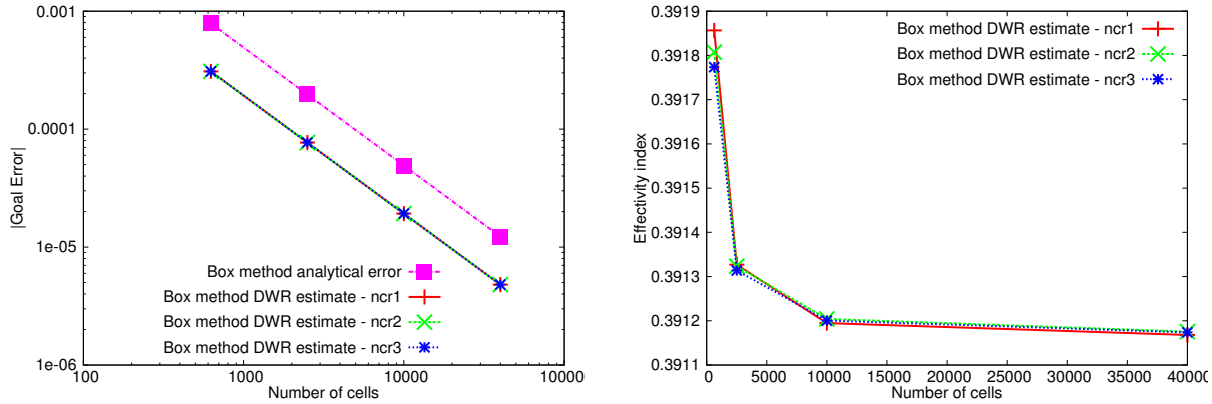

(a) Convergence (b) Effectivity index

Figure 11: Test case 3b results.

Similar comments can be made for test case 3b (figure 11). However, in this case the underestimation of the error is less severe (less than a factor of 3). There is also not much difference between the error estimate given by DWRs computed with adjoint solutions calculated on more refined meshes. This suggests that the remaining error is due to the non-linear terms.

5.4. Test case 4

This test case is a variation on the mini-BWR test case found in Taylor's thesis (Taylor, 2007). The geometry in (Taylor, 2007) is reflected in the x and y axis to produce the geometry of figure 12. 121 copies of the lattice geometry described in figure 12 are then placed in a 11×11 configuration. The boundary conditions of this larger geometry are then set to vacuum. The QoI in this test case is the K_{eff}. Reference results for this test case were provided via the AVARIS code (Kópházi, 2016), using a highly refined DGFEM mesh and the same angular quadrature. This test case was chosen to provide a more realistic problem to test the use of DWR error estimators on eigenvalue problems.

This test case is bigger, with less leakage and has a high scatter ratio throughout, thus the results are improved compared to the other eigenvalue test cases (section 5.3). The size of the problem means that the accuracy of results of the AVARIS code may be limited to some extent. However, the results given by the DWR error estimators give results that are no more than a factor of 2 away from the reference error (see figure 13).

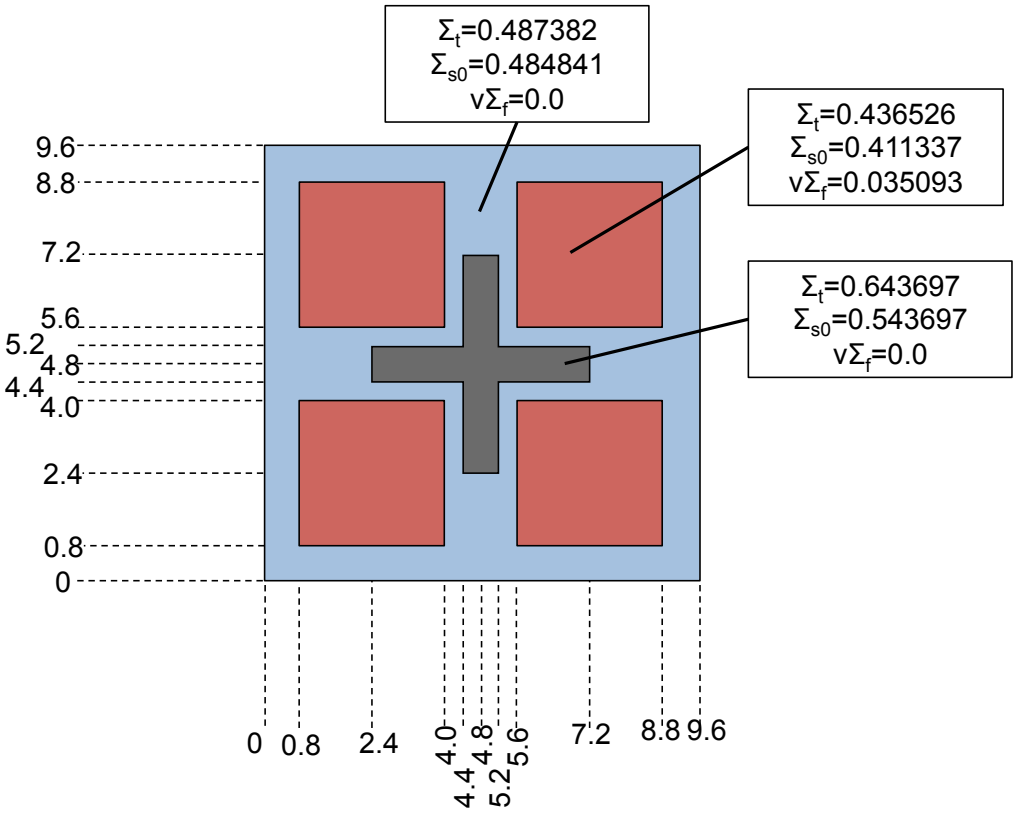

Figure 12: 2-D-Mini-BWR geometry and material property definition.

6. Goal-based AMR in 2-D for the DD scheme

Non goal based h AMR has been applied to the multi-dimensional DD scheme (Aussourd, 2003; Baker, 2002). h, p and hp DWR driven AMR has been applied to the 1-D DD scheme (Jeffers et al., 2017; Jeffers, 2017). However, extending the current work to provide multi-dimensional h AMR for the DD scheme driven by DWR error indicators would not be trivial. The WR theory behind the box method (and the equivalent DD method) breaks down with the addition of hanging nodes.

Figure 14 shows a hanging node between cell 1 and its two neighbouring cells (cells 2 and 4). For an ordinate that has a positive component going from left to right, the hanging node value could simply take the value given by the linear variation along the eastern cell edge of cell 1. However, the situation is not as clearcut if the component of the flux is going in the opposite direction (from a more refined region to a less refined region). Unless the hanging node happens to take a value that is exactly half the value of the nodes either side in the vertical direction, the condition of continuity along the line will not be satisfied. This means that the approximation will not exist in a subset of $(H_b^1)^{\frac{N(N+2)}{2}}$ and thus the WR theory behind the box method will break down.

One could allow for discontinuity in the solution, thereby making the calculation of the DWR similar to the case where we assume the bilinear term is zero (section 4.2). However, the equivalence between the cell-averaged values of the resulting solution and a WR scheme is lost, thereby making the DWR theory applied to the result more questionable than when the bilinear term was simply ignored (in section 4.2). Even if the vertex values are the DoF being solved for, flux values for the two right hand nodes of cell 1 (of figure 14) cannot be allocated in a unique manner. One could simply take the values at the nodes for the previous cells in the sweep and ignore the result on the hanging node. However, this would result in a lack of conservation of neutrons. One could ensure conservation of neutrons, but the issue of discontinuity and the lack of equivalence with a WR scheme remains.

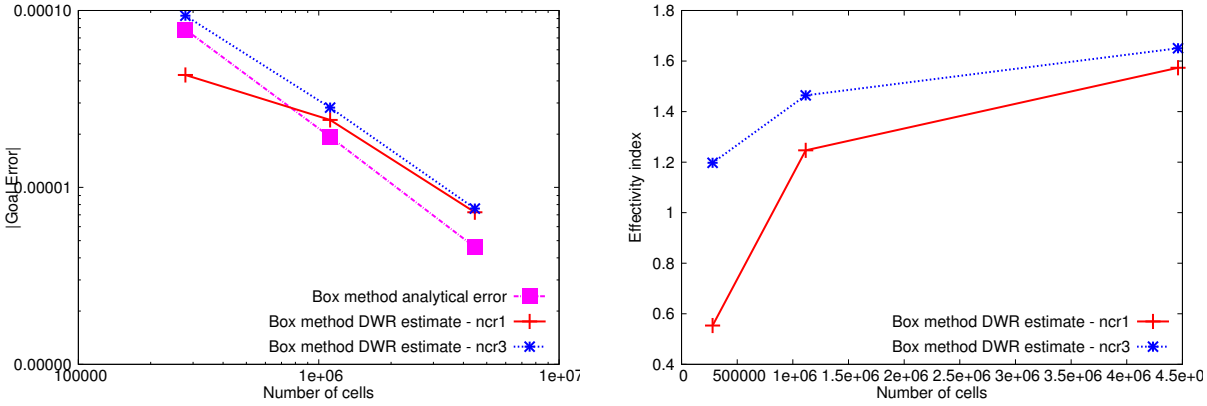

(a) Convergence

(b) Effectivity index

Figure 13: Test case 4 results.

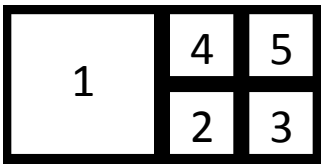

Figure 14: 2-D hanging node example

7. 3-D DWR methods for the DD and box method

The arguments in this paper have been presented for 2-D problems and applied to 2-D test cases. Similar arguments can be made for the 3-D test case.

The equivalent to the box method in 2-D can be found in the 3-D case by taking cells to be simply connected rectangular prisms and keeping the unknowns as the flux value at each vertex of the prism. A result in H^1 that is uniquely determined by cell vertex values results in a trilinear variation of the flux within the cell. This results in 8 parameters per cell, 7 of which are provided by the continuity condition between cells or by external boundary conditions (set by the fact that a solution in H^1 is sought). The remaining parameter is determined by a WR equation where the test functions are taken from a subset of L^2: piecewise constant function over the cell. Using the node numbering shown in figure 15, a trial function can be associated with each vertex in the cell:

$$N_1 = \frac{1}{8}(1-\zeta)(1-\gamma)(1+\omega) \tag{51}$$

$$N_2 = \frac{1}{8}(1+\zeta)(1-\gamma)(1+\omega) \tag{52}$$

$$N_3 = \frac{1}{8}(1+\zeta)(1+\gamma)(1+\omega) \tag{53}$$

$$N_4 = \frac{1}{8}(1-\zeta)(1+\gamma)(1+\omega) \tag{54}$$

$$N_5 = \frac{1}{8}(1-\zeta)(1-\gamma)(1-\omega) \tag{55}$$

$$N_6 = \frac{1}{8}(1+\zeta)(1-\gamma)(1-\omega) \tag{56}$$

$$N_7 = \frac{1}{8}(1+\zeta)(1+\gamma)(1-\omega) \tag{57}$$

$$N_8 = \frac{1}{8}(1-\zeta)(1+\gamma)(1-\omega) \tag{58}$$

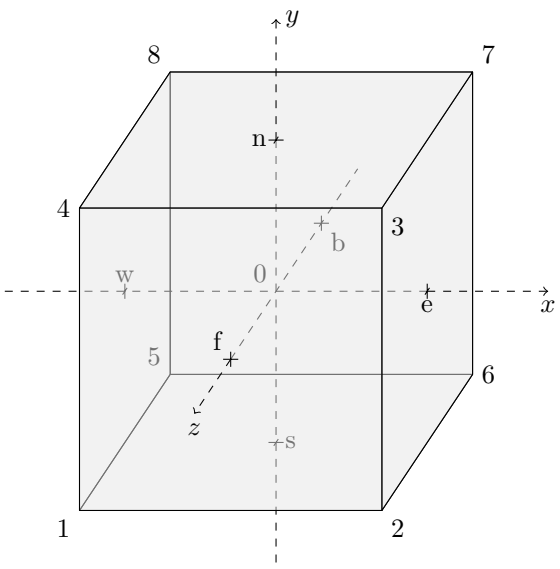

Figure 15: Node numberings for a rectangular prism

where:

$$\zeta = \frac{2x - x_w - x_e}{x_e - x_w}, \quad \gamma = \frac{2y - y_s - y_n}{y_n - y_s}, \quad \omega = \frac{2z - z_b - z_f}{z_f - z_b}. \tag{59}$$

Where w, e, n, s, represent the west, east, north and south faces (as in 2-D, but now the face is a rectangular area rather than a straight line). f and b represent the faces that are in the z direction towards the inside of the page and towards the outside of the page respectively.

The function within a cell can be represented in 2 ways, as in the 1-D and 2-D cases:

$$\Phi(x,y)_{\text{cell}} = \Phi(\zeta,\gamma) = \Phi_1 N_1 + \Phi_2 N_2 + \Phi_3 N_3 + \Phi_4 N_4 + \Phi_5 N_5 + \Phi_6 N_6 + \Phi_7 N_7 + \Phi_8 N_8 \tag{60}$$

and

$$\Phi(x,y)_{\text{cell}} = \Phi(\zeta,\gamma) = c_1 + c_2\zeta + c_3\gamma + c_4\omega + c_5\zeta\gamma + c_6\zeta\omega + c_7\omega\gamma + c_8\zeta\gamma\omega. \tag{61}$$

The WR equation obtained is as follows:

$$\frac{\mu}{4\Delta x_{ijk}}\left(\Phi_2 + \Phi_3 + \Phi_6 + \Phi_7 - \Phi_1 - \Phi_4 - \Phi_5 - \Phi_8\right) \tag{62}$$

$$+ \frac{\eta}{4\Delta y_{ijk}}\left(\Phi_3 + \Phi_4 + \Phi_7 + \Phi_8 - \Phi_1 - \Phi_2 - \Phi_5 - \Phi_6\right) \tag{63}$$

$$+ \frac{\xi}{4\Delta z_{ijk}}\left(\Phi_1 + \Phi_2 + \Phi_3 + \Phi_4 - \Phi_5 - \Phi_6 - \Phi_7 - \Phi_8\right) \tag{64}$$

$$+ \frac{\Sigma_{t,ijk}}{8}\sum_{v=1}^{8}\Phi_v = q_{ijk} \tag{65}$$

Grouping appropriate terms together gives the traditional representation of the DD method in 3-D:

$$\frac{\mu}{\Delta x_{ijk}}\left(\Phi_e - \Phi_w\right) + \frac{\eta}{\Delta y_{ijk}}\left(\Phi_n - \Phi_s\right) + \frac{\xi}{\Delta z_{ijk}}\left(\Phi_f - \Phi_b\right) + \Sigma_{t,ijk}\Phi_c = q_{ijk} \tag{66}$$

However, from these unknowns, the final 4 terms of the within cell flux approximation in equation (61) cannot be reconstructed. This means that the gap between the answer of the vertex method DWR and the version where the solution is mapped into a discontinuous FE space with the unknown terms artificially set to zero will be even worse in 3-D compared to 2-D. This is further motivation for calculating the vertex values as unknowns in industrial codes, rather than the cell-averaged and cell face-averaged fluxes.

8. Conclusions

This paper extended the 1-D WR view of the DD equation to 2-D to give the *box method* where the vertices of the cells are kept as unknowns. These unknowns can be collected together to give the traditional 2-D DD equations. The WR view of the DD equations in 2-D assumes a solution in H^1 with bilinear variation of the flux approximation within the cell. When the unknowns solved for are the cell-averaged and edge-averaged fluxes (such as in traditional implementations of DD codes) however, it is impossible to re-construct the bilinear term without taking the boundary condition and sweeping through the whole domain again. It is for this reason that 2 codes were written, one implementing the traditional box method and the other implementing the traditional DD equations. In the former, the DWR was calculated using the resulting piece-wise bilinear flux distribution that is uniquely determined by the cell vertex flux values. In the latter, the result was mapped into a bilinear DGFEM space where the bilinear term is artificially set to zero.

A possible higher order extension of the box method was suggested and its equivalence to the higher order Hébert method demonstrated mathematically. However this was not explored empirically.

The DWR error estimates calculated using the vertex unknowns gave very good results for fixed source high c problems. This was due to the increased stability and the lack of oscillations in the result when c is large. PWRs operate with large c values, thus suggesting that the *box method* DWR estimates could be appropriate for fixed source industrial cases.

The results for eigenvalue problems were less successful than for the fixed source case. Though, in the more realistic example that had reduced leakage and high scatter ratios, the effectivity index of the box method was within a factor of 2 of unity. An opportunity for future work would be to investigate ways of estimating the magnitude of the error terms not taken into account in the DWR for non-linear problems. Such work could investigate whether the results observed for the eigenvalue test cases in this chapter could be improved.

Assuming nc_x denotes the number of cells in the x direction and nc_y denotes the number of cells in the y direction, the number of unknowns per ordinate would be equal to $nc_x nc_y + nc_x + nc_y + 1$ if vertex values were stored, as opposed to $2nc_x nc_y + nc_x + nc_y$ if cell edge values were stored. However, it is often only the cell center values that are stored between iterations in traditional DD schemes (which requires $nc_x nc_y$ values).

A brief discussion on how these methods can be extended to 3-D test cases was provided. The theory shows that the advantages of solving for the vertex values in 3-D could be more significant than in 2-D.

Applying DWR driven AMR in 2-D would be more challenging than in the 1-D case due to the presence of the hanging nodes. Some of the theoretical challenges were discussed in section 6.

Acknowledgements

Dr. R.S. Jeffers would like to thank EPSRC for their support through the EPSRC grant Industrial Doctorate Centre: Nuclear Engineering (EPSRC grant number: EP/G037426/1) as well as EDF R&D for their industrial support. Dr. M.D. Eaton and Dr. J. Kophazi would like to thank EPSRC for their support through the following grants: Adaptive Hierarchical Radiation Transport Methods to Meet Future Challenges in Reactor Physics (EPSRC grant number: EP/J002011/1) and RADIANT: A Parallel, Scalable, High Performance Radiation Transport Modelling and Simulation Framework for Reactor Physics, Nuclear Criticality Safety Assessment and Radiation Shielding Analyses (EPSRC grant number: EP/K503733/1).

References

Nathan H. Hart and Yousry Y. Azmy. A residual-based a posteriori estimator of the spatial approximation error for discrete ordinates solutions of the transport equation. In *M&C 2017 - International Conference on Mathematics & Computational Methods Applied to Nuclear Science & Engineering*, 2017.

Salli Moustafa, Ivan Dutka-Malen, Laurent Plagne, Angélique Ponçot, and Pierre Ramet. Shared memory parallelism for 3D Cartesian discrete ordinates solvers. *Annals of Nuclear Energy*, 82:179 – 187, 2015. ISSN 0306-4549. doi: http://dx.doi.org/10.1016/j.anucene.2014.08.034. URL `http://www.sciencedirect.com/science/article/pii/S0306454914004265`. Joint International Conference on Supercomputing in Nuclear Applications and Monte Carlo 2013, SNA + MC 2013. Pluri- and Trans-disciplinarity, Towards New Modeling and Numerical Simulation Paradigms.

NEA. PARTISN 4.00: 1-D, 2-D, 3-D Time-Dependent, Multigroup Deterministic Parallel Neutral Particle Transport Code. Web, 2009. URL `http://www.oecd-nea.org/tools/abstract/detail/ccc-0707`. CCC-0707 PARTISN 4.00.

Thomas M. Evans, Alissa S. Stafford, Rachel N. Slaybaugh, and Kevin T. Clarno. Denovo: A new three-dimensional parallel discrete ordinates code in scale. *Nuclear Technology*, 171:171–200, August 2010.

Wolfgang Bangerth and Rolf Rannacher. *Adaptive Finite Element Methods for Differential Equations*. Lectures in Mathematics ETH Zürich. Birkhäuser Verlag, 2003.

D. Lathouwers. Goal-oriented spatial adaptivity for the S_N equations on unstructured triangular meshes. *Annals of Nuclear Energy*, 38(6):1373–1381, 2011a. ISSN 0306-4549. doi: 10.1016/j.anucene.2011.01.038. URL `http://www.sciencedirect.com/science/article/pii/S0306454911000594`.

D. Lathouwers. Spatially adaptive eigenvalue estimation for the S_N equations on unstructured triangular meshes. *Annals of Nuclear Energy*, 38(9):1867–1876, 2011b. ISSN 0306-4549. doi: 10.1016/j.anucene.2011.05.013. URL `http://www.sciencedirect.com/science/article/pii/S0306454911002039`.

Yaqi Wang and Jean C. Ragusa. Standard and goal-oriented adaptive mesh refinement applied to radiation transport on 2-D unstructured triangular meshes. *Journal of Computational Physics*, 230(3):763–788, 2011. ISSN 0021-9991. doi: 10.1016/j.jcp.2010.10.018. URL `http://www.sciencedirect.com/science/article/pii/S0021999110005747`.

Krzysztof J. Fidkowski and David L. Darmofal. Review of output-based error estimation and mesh adaptation in computational fluid dynamics. *AIAA Journal*, 49(4):673–694, 2011.

Niles A. Pierce and Michael B. Giles. Adjoint recovery of superconvergent functionals from PDE approximations. *SIAM REVIEW*, 42(2):247–264, 2000.

M.B. Giles, N.A. Pierce, and E. Süli. Progress in adjoint error correction for integral functionals. *Comput Visual Sci*, 6:113–121, 2004.

Qingshan Chen and Max Gunzburger. Goal-oriented a posteriori error estimation for finite volume methods. *Journal of Computational and Applied Mathematics*, 265:69–82, 2014.

David A. Venditti and David L. Darmofal. Grid adaptation for functional outputs: Application to two-dimensional inviscid flows. *Journal of Computational Physics*, 176:40–69, 2002.

Jose I. Duo, Yousry Y. Azmy, and Ludmil T. Zikatanov. A posteriori error estimator and AMR for discrete ordinates nodal transport methods. *Annals of Nuclear Energy*, 36(3):268 – 273, 2009. ISSN 0306-4549. doi: http://dx.doi.org/10.1016/j.anucene.2008.12.008. URL `http://www.sciencedirect.com/science/article/pii/S0306454908003368`. PHYSOR 2008.

Juhani Pitkäranta. On the spatial differencing of the discrete ordinate neutron transport equation. *SIAM J. Numerical Analysis*, 15:859–869, 1978.

R.S. Jeffers, J. Kópházi, M.D. Eaton, F. Févotte, F. Hülsemann, and J. Ragusa. Goal-based h-adaptivity of the 1-d diamond difference discrete ordinate methods. *Journal of Computational Physics*, 335:179 – 200, 2017. ISSN 0021-9991. doi: http://dx.doi.org/10.1016/j.jcp.2017.01.037. URL //www.sciencedirect.com/science/article/pii/S0021999117300530.

R.S. Jeffers. Spatial Goal-Based Error Estimation and Adaptive Mesh Refinement (AMR) for Diamond Difference Discrete Ordinate (DD-S_N) Methods, 2017. EngD Thesis. Imperial College London.

E.E. Lewis and Jr. W.F. Miller. *Computational Methods of Neutron Transport*. American Nuclear Society Inc., 1993.

Alain Hébert. High order diamond differencing schemes. *Annals of Nuclear Energy*, 33:1479–1488, 2006.

Nicolas Martin and Alain Hébert. A three-dimensional S_N high-order diamond differencing discretization with a consistent acceleration scheme. *Annals of Nuclear Energy*, 36:1787–1796, 2009.

Dimitris Valougeorgis. Boundary treatment of the diffusion synthetic acceleration method for fixed-source discrete-ordinates problems in x-y geometry. *Nuclear Science and Engineering*, 100:142–148, 1988.

Christian Aussourd. Styx: A multi-dimensional AMR S_N schemes. *Nuclear Science and Engineering*, 143: 281–290, 2003.

Randal S. Baker. A block adaptive mesh refinement algorithm for the neutral particle transport equation. *Nuclear Science and Engineering*, 141:1–12, 2002.

Claes Johnson and Juhani Pitkäranta. Convergence of a fully discrete scheme for two-dimensional neutron transport. *SIAM J. Numer. Anal.*, 20(5):951–966, 1983.

Yaqi Wang and Jean C. Ragusa. On the Convergence of DGFEM Applied to the Discrete Ordinates Transport Equation for Structured and Unstructured Triangular Meshes. *Nuclear Science and Engineering*, 163:56–72, 2009.

R. Le Tellier and A. Hébert. A modeling of BWR-MOX assemblies based on the characteristics method combined with advanced self-shielding Models. *Nuclear Science and Engineering*, 158:231–243, 2008.

Weston M. Stacey. *Nuclear Reactor Physics*. Wiley-Vch, 2007.

J. I. Duo and Y. Y. Azmy. Error comparison of diamond difference, nodal, and characteristic methods for solving multidimensional transport problems with the discrete ordinates approximation. *Nuclear Science and Engineering*, 156:139–153, 2007.

Jose Ignacio Duo. *Error estimates for nodal and short characteristics spatial approximations of two-dimensional discrete ordinates methods*. PhD thesis, The Pennsylvania State University, May 2008.

William H. Reed. New difference schemes for the neutron transport equation. *Nuclear Science and Engineering*, 36:309–314, 1971.

Edward W. Larsen. Spatial convergence properties of the diamond difference method in x,y geometry. *Nuclear Science and Engineering*, pages 710–713, 1981.

J.I. Duo and Y.Y. Azmy. Spatial convergence study of discrete ordinates methods via the singular characteristic tracking algorithm. *Nuclear Science and Engineering*, 162:41–55, 2009.

Alain Hébert. *Applied Reactor Physics*. Presses Internationales Polytechnique, 2010.

Thomas J.R. Hughes. *The Finite Element Method. Linear Static and Dynamic Finite Element Analysis*. Dover, 2000.

J. P. Hennart and E. del Valle. A generalized nodal finite element formalism for discrete ordinates equations in slab geometry: Part I: Theory in the continuous moment case. *Transport Theory and Statistical Physics*, 24:449–478, 1995.

J.P. Hennart and E del Valle. On nodal transport methods. Technical Report 2947, INRIA, July 1996.

J. Kópházi. AVARIS neutron transport code. Rolls-Royce, 2016. Code written and all test cases using this code completed by J. Kópházi.

J. Stepanek, T. Auerbach, and W. Halg. Calculation of four thermal reactor benchmark problems in x-y geometry. Technical Report 464, Federal Institute of Technology Zurich, 1982.

James Bryce Taylor. *The development of a three-dimensional nuclear reactor kinetics methodology based on the method of characteristics*. PhD thesis, The Pennsylvania State University, 2007.